

REPORT ON PROGRESS

Strong-laser-field physics, non-classical light states and quantum information science

To cite this article: U Bhattacharya *et al* 2023 *Rep. Prog. Phys.* **86** 094401

View the [article online](#) for updates and enhancements.

You may also like

- [Non-classical light in a \$J_x\$ photonic lattice](#)

Manoranjan Swain and Amit Rai

- [Quantum metrology of solid-state single-photon sources using photon-number-resolving detectors](#)

Martin von Helversen, Jonas Böhm, Marco Schmidt et al.

- [Multidimensional spectroscopy with entangled light: loop vs ladder delay scanning protocols](#)

Konstantin E Dorfman and Shaul Mukamel

Report on Progress

Strong–laser–field physics, non–classical light states and quantum information science

U Bhattacharya¹, Th Lamprou^{2,3}, A S Maxwell⁴ , A Ordóñez¹ , E Pisanty⁵ , J Rivera-Dean¹ , P Stammer¹ , M F Ciappina^{6,7,8} , M Lewenstein^{1,9}  and P Tzallas^{2,10,*} 

¹ ICFO-Institut de Ciències Fotoniques, The Barcelona Institute of Science and Technology, Castelldefels (Barcelona) 08860, Spain

² Foundation for Research and Technology-Hellas, Institute of Electronic Structure & Laser, GR-70013 Heraklion (Crete), Greece

³ Department of Physics, University of Crete, PO Box 2208, GR-71003 Heraklion (Crete), Greece

⁴ Department of Physics and Astronomy, Aarhus University, DK-8000 Aarhus C, Denmark

⁵ Attosecond Quantum Physics Laboratory, Department of Physics, King's College London, Strand WC2R 2LS, London, United Kingdom

⁶ Department of Physics, Guangdong Technion—Israel Institute of Technology, 241 Daxue Road, Shantou, Guangdong 515063, People's Republic of China

⁷ Technion—Israel Institute of Technology, Haifa 32000, Israel

⁸ Guangdong Provincial Key Laboratory of Materials and Technologies for Energy Conversion, Guangdong Technion—Israel Institute of Technology, 241 Daxue Road, Shantou 515063, Guangdong, People's Republic of China

⁹ ICREA, Pg. Lluís Companys 23, 08010 Barcelona, Spain

¹⁰ ELI ALPS, ELI-HU Non-Profit Ltd, Wolfgang Sandner utca 3., Szeged H-6728, Hungary

E-mail: ptzallas@iesl.forth.gr

Received 14 February 2023, revised 6 July 2023

Accepted for publication 25 July 2023

Published 7 August 2023

Corresponding editor: Dr Masud Mansuripur



Abstract

Strong–laser–field physics is a research direction that relies on the use of high-power lasers and has led to fascinating achievements ranging from relativistic particle acceleration to attosecond science. On the other hand, quantum optics has been built on the use of low photon number sources and has opened the way for groundbreaking discoveries in quantum technology, advancing investigations ranging from fundamental tests of quantum theory to quantum information processing. Despite the tremendous progress, until recently these directions have remained disconnected. This is because the majority of the interactions in the strong-field limit have been successfully described by semi-classical approximations treating the electromagnetic field classically, as there was no need to include the quantum properties of the field to explain the observations. The link between strong–laser–field physics, quantum optics, and quantum information science has been developed in the recent past. Studies based on fully quantized and conditioning approaches have shown that intense laser–matter interactions can be used for the generation of controllable entangled and non-classical light states. These achievements open the

* Author to whom any correspondence should be addressed.

way for a vast number of investigations stemming from the symbiosis of strong–laser–field physics, quantum optics, and quantum information science. Here, after an introduction to the fundamentals of these research directions, we report on the recent progress in the fully quantized description of intense laser–matter interaction and the methods that have been developed for the generation of non-classical light states and entangled states. Also, we discuss the future directions of non-classical light engineering using strong laser fields, and the potential applications in ultrafast and quantum information science.

Keywords: quantum optics, quantum electrodynamics, quantum light, quantum information, strong laser physics, high harmonic generation

(Some figures may appear in colour only in the online journal)

Contents

1. Introduction	2	5.1.2. Detection of strongly correlated systems with HHG	20
2. Fundamentals of QO and non-classical light engineering	4	5.1.3. Detection of chirality with HHG	21
2.1. Quantum harmonic oscillator	4	5.2. Generation of topology, strongly correlated systems, chirality, etc	22
2.2. Coherent states of light	4	5.3. Strong-field physics and atto-second science driven by non-classical light	23
2.3. Quantum state characterization	4	5.4. Generation of entanglement in <i>Zerfall</i> processes	23
2.4. Non-classical light states	6	5.5. Characterizing decoherence in <i>Zerfall</i> processes	23
2.4.1. Photon number (Fock) states	6	6. Conclusions	24
2.4.2. Squeezed light states	6	Data availability statement	24
2.4.3. CSs and optical ‘cat’ states	6	Acknowledgments	24
2.4.4. Entangled states	7	References	25
3. Fundamentals of intense laser-matter interactions: semi-classical approaches	8		
3.1. Intense laser–atom interaction	8		
3.1.1. ATI and HATI	8	1. Introduction	
3.1.2. HHG	10		
3.1.3. Non-sequential double ionization (NSDI)	10	Until the end of the ’50s, natural (incoherent) light was	
3.1.4. The strong field approximation	10	the main available source, with a well-formulated quantum	
4. Intense laser–atom interaction: fully quantized approach	11	description, that had been successfully used in the majority	
4.1. QED of intense laser–atom interactions	11	of investigations exploiting light–matter interactions. Because	
4.1.1. Conditioning on HHG using single–color driving fields: generation of optical ‘cat’ and entangled states from XUV to IR	11	of this, the quantum description of a classically oscillating	
4.1.2. Conditioning on HHG using two–color driving fields: generation of optical ‘cat’ and entanglement between the driving field modes	12	electromagnetic field (as given by classical electrodynamics)	
4.1.3. Conditioning on ATI and generation of optical ‘cat’ states	12	remained unexploited. This changed at the end of ’50s and	
4.2. Experimental approach: Generation of optical ‘cat’ states	17	the beginning of ’60s with three groundbreaking discoveries:	
4.2.1. Controlling the quantum features of the optical ‘cat’ states	17	the Hanbury Brown and Twiss experiment (conducted using incoherent light) [1], the laser invention by T H	
4.3. Extension to interactions with complex materials and generation of massively entangled states	18	Maiman (and earlier maser) (see [2] and references therein)	
5. Applications in QI science	19	and the formulation of the quantum theory of optical coherence	
5.1. Detection of topology, strongly correlated systems, chirality, etc	20	and the invention of coherent states of light (used for the	
5.1.1. Detection of topological order with HHG	20	description of a classically oscillating field) by Roy Glauber	
		and George Sudarshan (see [3–5]). These achievements were	
		poised to drastically speed up scientific progress and provide	
		countless revolutionary discoveries moving from Nobel-prize	
		winning experiments, into cross-disciplinary fields of basic	
		research and technology [6–21]. This scientific progress is	
		largely based on the development of the research directions of	
		quantum optics (QO), and strong–laser–field physics (SLP).	
		The latter by making possible the progress in laser technology	
		and especially in pulsed laser sources [17, 18].	
		In particular, QO is based on the quantum description of	
		the electromagnetic radiation and largely on the formulation	
		of the quantum theory of optical coherence [3–5, 22–24].	
		A key aspect is the measurement of light intensity fluctuations	

and the characterization of the quantum state of the electromagnetic field, typically achieved by photon statistics measurements, the measurement of photon correlation functions [1, 3, 4, 25], and by means of quantum tomography methods [26–32]. In the case of light–matter interaction, the majority of the studies are performed using weak electromagnetic fields (low photon number light sources) where the interaction is described by fully quantized theories, with the research, for many years, being focused on single or few body phenomena, trying to understand non-perturbative aspects of atom–light interaction (for a recent overview see [33]).

QO is at the core of quantum technologies [34–36]. This is because light is considered as an ideal resource for engineering quantum states (such as squeezed, Fock, optical Schrödinger ‘cats’) [14, 15, 19–21, 25, 26, 37–53] with non-classical properties. These light states have some very distinct features and advantages compared to classical light. They can provide reduced noise and the notable feature of quantum correlations. Furthermore, light does not suffer as much from decoherence, in comparison to matter particles, when scaling to macroscopic sizes. This is because the electromagnetic environment at optical frequencies can be considered as vacuum (i.e. as an environment with no particles) and thus relatively decoherence-free. These notable properties made non-classical light a key element for the emergence of new quantum technologies. Nowadays, the generation of non-classical and entangled light states has a vital role in quantum technologies as they offer a unique resource in a vast variety of investigations in quantum information (QI) science ranging from fundamental tests of quantum theory, quantum sensing, teleportation, communication, cryptography, visual science to high-precision interferometry applied for the detection of gravitational waves [14, 15, 19–21, 34–36, 54–61]. However, despite the progress achieved so far, the applicability of the majority of the existing non-classical light sources is restricted by their low photon number, while the development of new schemes for the generation of high photon number non-classical and entangled light states is considered challenging.

On the other hand, SLP relies on the use of strong laser fields and largely on models employing semi-classical approximations, where the electromagnetic field is treated classically. The enhancement of laser power came almost a decade after the laser invention [62], with the development of nanosecond (ns) and picosecond (ps) pulsed laser sources [63, 64]. By using these sources, the observation of nonlinear processes was made possible. Due to the relatively low electric field of these laser pulses (compared to the Coulomb field of the atomic potential), these interactions were successfully described by the lowest-order perturbation theory (LOPT) using multi-photon absorption processes [65]. At the end of 80s, the development of femtosecond (fs) [66, 67] pulsed laser sources, combined with the pioneer development of the chirped-pulse amplification technique [17, 18], opened the way for time-resolved experiments in molecules

[68] and investigations beyond the perturbative regime. In particular, high-power fs lasers allowed the scientific community to explore non-linear interactions in the strong field limit where the laser-electric field strength is comparable to, or even stronger than, the atomic potential [69–72]. Such interactions have opened the way for studies ranging from relativistic particle acceleration ([17] and references therein), to high harmonic generation (HHG) [73, 74], high-resolution spectroscopy in the extreme ultraviolet (XUV) [75, 76] and attosecond physics (AP) [77–82]. The interaction of atoms with strong laser pulses is at the core of the investigations in SLP and ultrafast science. Central to these studies, is the process of HHG where the low frequency photons of a driving laser pulse, after the interaction with atoms, are up-converted into photons of higher frequencies in the XUV spectral range. These interactions have been successfully described by classical or semi-classical strong field approximations, namely the three-step model [70–72, 83], treating the electromagnetic field classically and ignoring its quantum nature. Because of this, advantages emerging from the connection of QO with SLP remained unexploited. By connecting QO with SLP, we can start answering the following fundamental questions: (a) *What is the back-action of the interaction on the driving field?* and (b) *What is the quantum state of the radiation after the interaction with matter?* The importance of providing an answer to these two questions is directly associated with the applicability of SLP to quantum technologies. Several groups have provided early attempts towards this direction [84–97]. However, despite the important information provided by these studies, none of these efforts have addressed the above questions. This has recently changed. Theoretical and experimental investigations [52, 53, 98], conducted using fully quantized approaches in the strong-field limit, have linked SLP and ultrafast science with QO. This has been achieved by showing that the intense laser-matter interactions and conditioning approaches [99–102] on the process of high-harmonic generation, can be used for the generation of high photon number non-classical and entangled light states with controllable quantum features [53, 98, 103–105]. These notable properties can be used for the development of a new class of non-classical and entangled states, advancing investigations in quantum technologies.

Here, after an introduction to the fundamentals of QO and intense laser–matter interactions, we will discuss a fully quantized description of the latter. We will put emphasis on quantum electrodynamics (QED) of intense laser–atom interactions and the methods developed for engineering high photon number non-classical and entangled light states with controllable quantum features. Then, we will provide potential directions and recent investigations towards the generation of non-classical light states using strongly laser-driven complex materials, and finally we will discuss the generation of high photon number non-classical and massively entangled light states and the potential applications in ultrafast and QI science.

2. Fundamentals of QO and non-classical light engineering

QO is a major research direction in the area of atomic, molecular and optical physics, which has been discussed in an enormous amount of books and articles published over the years (see [22–24, 106–109]). Here, for reasons of completeness and for introducing the terminology and definitions relevant to the present article, we will discuss a few of the fundamentals of this research direction.

2.1. Quantum harmonic oscillator

The foundations of QO are based on the quantization of the electromagnetic field which, when expanded into its frequency modes, can be written as a set of independent quantum harmonic oscillators (see [23, 106, 108] for a detailed derivation), each of them having a frequency ω . Thus, for a single mode, we can write the corresponding Hamiltonian as $\hat{H} = \frac{1}{2}(\hat{p}^2 + \omega^2\hat{x}^2) = \hbar\omega(\hat{a}^\dagger\hat{a} + 1/2)$, where \hat{x} and \hat{p} are the canonical operators of the harmonic oscillator, analog to the position and momentum operators of a particle in a harmonic potential, which satisfy the commutation relation $[\hat{x}, \hat{p}] = i\hbar$; and $\hat{N} = \hat{a}^\dagger\hat{a}$ is the photon number operator, with \hat{a}^\dagger and \hat{a} the creation and annihilation operators, respectively, which satisfy $[\hat{a}, \hat{a}^\dagger] = 1$. The canonical variables \hat{x} and \hat{p} are related to the creation and annihilation operators by $\hat{x} = \sqrt{\hbar/(2\omega)}(\hat{a} + \hat{a}^\dagger)$ and $\hat{p} = i\sqrt{\hbar\omega/2}(\hat{a}^\dagger - \hat{a})$. However, instead of working with the canonical variables \hat{x} and \hat{p} , in QO we usually work with dimensionless operators referred to as *quadrature operators*, \hat{x} and \hat{p} , which are related to the creation and annihilation operators as $\hat{x} = (\hat{a} + \hat{a}^\dagger)/\sqrt{2}$ and $\hat{p} = (\hat{a} - \hat{a}^\dagger)/(i\sqrt{2})$.

The eigenstates of the Hamiltonian presented before, are the so-called Fock states $|n\rangle$, with $n \in \mathbb{N}$ and eigenvalue $\hbar\omega(n + 1/2)$. Thus, since they are eigenstates of the photon number operator \hat{N} , Fock states (also known as photon number states) have a well-defined photon number. The state that has $n = 0$ photons, i.e. $|0\rangle$, defines the so-called *vacuum* state. In the quadrature x -representation, a Fock state can be written as $\langle x|n\rangle = \psi_n(x) = \psi_0(x)H_n(x)/\sqrt{2^n n!}$, where $H_n(x)$ is the n th-order Hermite polynomial and $\psi_0(x) = \exp(-x^2/2)/\pi^{1/4}$ is the wavefunction of the vacuum state.

Finally, the electric field operator corresponding to a single mode of the electromagnetic field is given by $\hat{E}(t) = \sqrt{\hbar\omega/(\epsilon_0 V)}(\hat{a}e^{-i\omega t} + \hat{a}^\dagger e^{i\omega t})$, with V the quantization volume and ϵ_0 the vacuum permittivity. In terms of the quadrature operators, it reads as $\hat{E}(t) = \sqrt{2\hbar\omega/(\epsilon_0 V)}(\cos(\omega t)\hat{x} + \sin(\omega t)\hat{p})$.

2.2. Coherent states of light

The quantum description of a classically oscillating field becomes feasible with the formulation of coherent states of light. A single-mode classical electromagnetic field is often described as a wave with a well-defined amplitude and phase. However, in the quantum theory of radiation, amplitude and phase are conjugate variables, and therefore cannot be determined with arbitrary accuracy in the same experiment. Coherent

(or Glauber) states of light, are states for which the product of the variances of these two quantities reaches its lower limit, i.e. the fluctuations in the two quadratures are equal, and minimize the uncertainty product given by Heisenberg's uncertainty relation $\Delta x\Delta p = \frac{1}{2}$ with $\Delta x = \Delta p = \frac{1}{\sqrt{2}}$. Therefore, coherent states provide the optimal description of a classical field. They are typically denoted as $|\alpha\rangle$, with Greek letters, and can be expanded in the Fock state basis as

$$|\alpha\rangle = e^{-|\alpha|^2/2} \sum_{n=0}^{\infty} \frac{\alpha^n}{\sqrt{n!}} |n\rangle, \quad (1)$$

with $\alpha = |\alpha| \exp(i\theta)$, the complex amplitude, such that the mean-photon number is given by $\langle n \rangle = \langle \alpha | \hat{N} | \alpha \rangle = |\alpha|^2$. These states are eigenstates of the annihilation operator, i.e. $\hat{a}|\alpha\rangle = \alpha|\alpha\rangle$, and can be generated by coupling a classically oscillating current, $\mathbf{J}(\mathbf{r}, t)$, to the vector potential operator of an electromagnetic field mode, $\hat{\mathbf{A}}(\mathbf{r}, t)$, so that the Hamiltonian describing the interaction is $\hat{H} = \int d^3 r \mathbf{J}(\mathbf{r}, t) \cdot \hat{\mathbf{A}}(\mathbf{r}, t)$. The unitary evolution associated to this Hamiltonian can be written in terms of the displacement operator $\hat{D}(\alpha) = \exp(\alpha\hat{a}^\dagger - \alpha^*\hat{a})$, which induces a shift in phase-space of the corresponding initial state, with the amplitude α proportional to the Fourier component of the classical current with respect to the mode with frequency ω . If, for instance, we consider the initial state to be the vacuum state $|0\rangle$, then we get a coherent state of amplitude α , i.e. $|\alpha\rangle = \hat{D}(\alpha)|0\rangle$. Equivalently, in terms of the quadrature representation, we can write $\alpha = (x_0 + ip_0)/\sqrt{2}$, with $x_0 = \langle \alpha | \hat{x} | \alpha \rangle$ and $p_0 = \langle \alpha | \hat{p} | \alpha \rangle$, the displacement operator as $\hat{D} = \exp(ip_0\hat{x} - ix_0\hat{p})$ and its wavefunction in the x -representation as $\langle x | \alpha \rangle = \psi_\alpha(x) = \psi_0(x - x_0) \exp(ip_0x - ip_0x_0/2)$, where $\psi_0(x - x_0) = \pi^{-1/4} e^{-(x-x_0)^2/2}$ is the wavefunction of the shifted vacuum state. The time-evolution of coherent states under free-field dynamics, i.e. dictated by the Hamiltonian $\hat{H} = \hbar\omega(\hat{a}^\dagger\hat{a} + 1/2)$, is given by $|\alpha(t)\rangle = \exp(-i\hat{H}t/\hbar)|\alpha\rangle = \exp(-i\omega t/2)|\alpha \exp(-i\omega t)\rangle$, from which it stems that coherent states remain coherent under free-field evolution. Thus, in the quadrature x -representation $\langle x | \alpha(t) \rangle = \psi_\alpha(x, t)$, the obtained wavefunction describes a Gaussian wavepacket, unchanged in time, which oscillates with the frequency of the field following a motion like a classical particle in a harmonic oscillator potential.

If, by using the above, we compute the expectation value of the electric field operator, we get $\langle \alpha | \hat{E}(t) | \alpha \rangle = |\alpha| \cos(\omega t - \theta)$, which is the expression of a monochromatic electromagnetic field obtained in classical electromagnetism. For this reason coherent states are referred to as ‘classical’ or ‘quasi-classical’. Fields described by a statistical mixture of coherent states, such as thermal fields, are considered as classical as well, while any state that cannot be described by this kind of mixtures is typically regarded as ‘non-classical’.

2.3. Quantum state characterization

The characterization of the quantum state of light is a large chapter in QO and it is practically impossible to fully address it in a single section of a manuscript. Some of the most useful

methods that are commonly used to characterize and distinguish the classical from the non-classical light fields are based on the measurement of the (I) q th order correlation functions $g^{(q)}(\tau)$ [3, 4, 11], (II) photon number distribution, and (III) Wigner function (or Q-, P-functions) in phase space [110]. Each of these methods alone is sufficient, but not necessary, to distinguish classical from non-classical light (for details see [111] and references therein).

In method (I), the $g^{(q)}$ functions are used (with $q = 2$ being the most commonly used) to characterize the statistics and the degree of coherence of an electromagnetic field. The $g^{(q)}(\tau)$ functions are typically obtained by interferometric approaches and q th order autocorrelation measurements, with q being the order of nonlinearity and τ the time delay between the photon signals. In method (II), the photon number distribution, given by $P_n = |\langle n|\psi \rangle|^2$ (where $|\psi\rangle$ is the quantum state of the field), can be obtained directly by photon statistics measurements. Regarding these methods, a coherent state depicts a Poissonian photon number distribution with $P_n = |\langle n|\alpha \rangle|^2 = e^{-|\alpha|^2} |\alpha|^{2n}/n! = e^{-\langle n \rangle} \langle n \rangle^n/n!$, and a normalized $g^{(2)}(0) = 1$. This refers to the case where photons randomly reach a detector. A light source is called super-Poissonian if the photon number distribution leads to $g^{(2)}(0) > 1$, and photon bunching is observed. This refers to the case where the photons have the tendency to reach the detector in bunches, i.e. more close in space (time) than the photons of the coherent state. It is noted that incoherent light also corresponds to this case with the photon number fluctuations to be determined by the coherence time of the light source. A non-classical light source with sub-Poissonian photon number distribution and $0 < g^{(2)}(0) < 1$, shows photon antibunching signatures. This is a pure quantum effect which refers to the case where the photons have the tendency to reach the detector more equally and further away in space (time) than those of a coherent state.

In method (III), the Wigner function can be obtained by implementing a homodyne detection technique and quantum tomography method [26–28]. This method is considered as one of the most complete ways of characterizing a light state. An optical layout of the technique, implemented by means of an interferometric approach, is shown in figure 1. E_{in} is the field of the state to be characterized. The E_{in} field in the 1st branch of the interferometer, is spatiotemporally overlapped on a beam splitter (BS) with the field of a local oscillator E_r (with $E_r \gg E_{in}$). The E_r field comes from the 2nd branch of the interferometer which introduces a controllable phase shift φ between the E_{in} and E_r fields. The fields after the BS are detected by a balanced differential photodetection system consisting of two identical photodiodes (PDs). This provides at each value of φ the photocurrent difference i_φ . The characterization of the quantum state of light can be achieved by recording the value of i_φ as a function of φ . These values are directly proportional to the measurement of the electric field operator $\hat{E}_{in}(\varphi) \propto \hat{x}_\varphi \propto \cos(\varphi)\hat{x} + \sin(\varphi)\hat{p}$ and are used for the reconstruction of the Wigner function via Radon transformation [112]. Experimentally, this is all that one has to do in order to characterize the light state. This is because repeated measurements of \hat{x}_φ at each φ provides the probability distribution

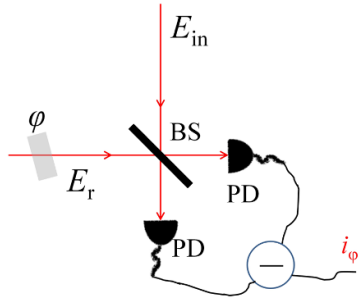


Figure 1. Homodyne detection and quantum tomography approach. E_{in} is the state of the field to be characterized, while E_r is the field of a local oscillator E_r (with $E_r \gg E_{in}$). BS is a beam splitter, and φ is the controllable phase shift between the E_{in} and E_r fields. Two identical photodiodes, labeled PD, use a balanced differential photodetection system, which provides, at each value of φ , the photocurrent difference i_φ . The characterization of the quantum state of light can be achieved by recording the value of i_φ as a function of φ .

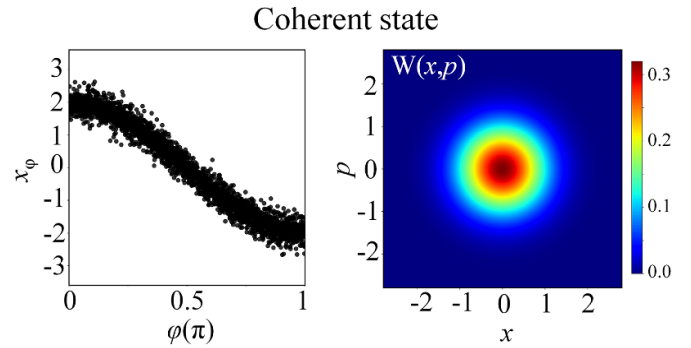


Figure 2. Homodyne trace and Wigner function of a coherent light state $|\alpha\rangle$. The left panel shows the calculated homodyne detection signal x_φ , and the right panel the corresponding Wigner function $W(x,p)$ which has been centered at $|\alpha| = 2$. Reproduced from [98]. CC BY 4.0.

$P_\varphi(x_\varphi) = \langle x_\varphi | \hat{\rho} | x_\varphi \rangle$ of its eigenvalues x_φ , where $\hat{\rho} \equiv |\phi\rangle\langle\phi|$ is the density operator of the light state to be characterized and $|x_\varphi\rangle$ the eigenstate with eigenvalue x_φ . The density matrix $\hat{\rho}$, which provides complete information about the light state, can be obtained in the Fock basis by calculating the matrix elements ρ_{nm} using an iterative *Maximum-Likelihood* procedure beautifully described in [113]. Having determined these values, the mean photon number of the light state can be obtained by the diagonal elements ρ_{nn} of the density matrix $\hat{\rho}$, and the relation $\langle n \rangle = \sum n \rho_{nn}$. Figure 2 shows a calculated homodyne trace (left panel) and the reconstructed Wigner function (right panel) of a coherent state. The Wigner function, which is the Wigner function of the vacuum state shifted by (x_0, p_0) , depicts a Gaussian distribution of the form $W(x,p) = \frac{1}{\pi} \exp[-(x - x_0)^2 - (p - p_0)^2]$ which in a more compact form reads,

$$W(\beta) = \frac{2}{\pi} e^{-2|\beta - \alpha|^2}. \quad (2)$$

In the above equation we have used the transformation $x \equiv \text{Re}[\beta - \alpha]$ and $p \equiv \text{Im}[\beta - \alpha]$ (where $\beta = (x + ip)/\sqrt{2}$ is a

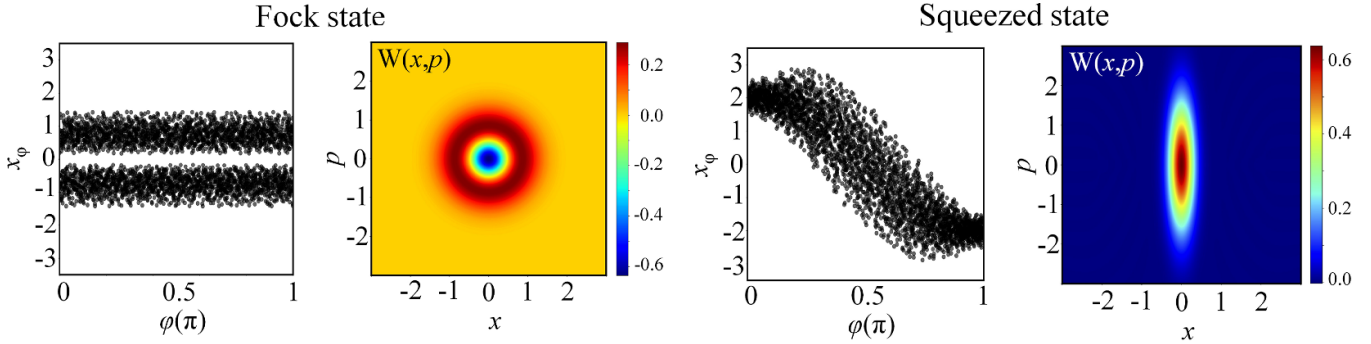


Figure 3. Homodyne trace and Wigner function of a Fock state $|n\rangle$ with $n = 1$. The left panel shows the calculated homodyne detection signal x_ϕ , and the right panel the corresponding Wigner function $W(x,p)$.

variable), which centers the Wigner function at the origin for $\beta = \alpha$, $x = 0$ and $p = 0$.

2.4. Non-classical light states

Any state that cannot be described by a mixture of coherent states, or provides a Wigner function that depicts negative values and/or non-Gaussian distributions, is considered non-classical. Such states include Fock states, squeezed states, and coherent state superpositions (CSSs), e.g. optical Schrödinger ‘cat’ states. Because these states are central to quantum technologies, in the following subsections we provide some of their main features.

2.4.1. Photon number (Fock) states. From an experimental perspective, Fock states are delivered by single-photon sources, which have been developed by means of single atom and molecule transitions [25, 114], ion-traps [42], defect centers in solid state materials [115, 116], quantum dots [43], 2D materials [117], etc. Nowadays, the most commonly used source is based on a non-linear parametric down-conversion process [44–47], where a high energy photon, after interacting with a non-linear medium, is converted into a pair of lower-energy photons. Fock states depict photon anti-bunching properties with a sub-Poissonian photon number distribution, confined at the photon number n . The Wigner function has a ring-shaped structure, centered at $(x = 0, p = 0)$, and depicts negative values. It has the form $W_n(x,p) = \frac{(-1)^n}{\pi} \exp(-x^2 - p^2) L_n(2x^2 + 2p^2)$ which, according to the transformation used in equation (2), reads

$$W_n(\beta) = \frac{2}{\pi} (-1)^n e^{-2|\beta|^2} L_n(4|\beta|^2), \quad (3)$$

where L_n are the n -order Laguerre polynomials. Figure 3 shows an example of a calculated homodyne trace (left panel) and the corresponding Wigner function (right panel) of the single photon Fock state $|1\rangle$.

2.4.2. Squeezed light states. In contrast to coherent states of light, quantum fluctuations for squeezed states of light are

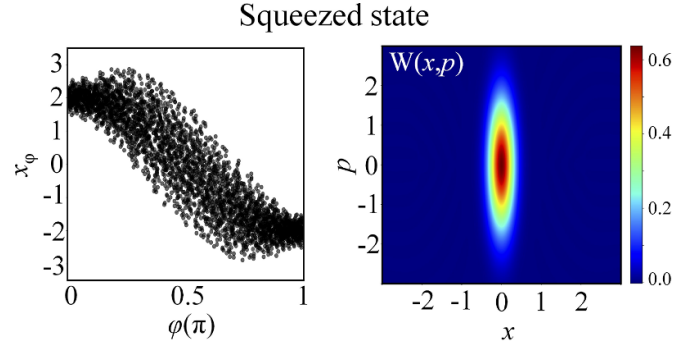


Figure 4. Homodyne trace and Wigner function of an amplitude squeezed state with $|\alpha| = 2$ and $k = 0.8$. The left panel shows the calculated homodyne detection signal x_ϕ , and the right panel the corresponding Wigner function $W(x,p)$ which has been centered at $|\alpha| = 2$.

not equally distributed between the field quadratures. They are minimum uncertainty states, which have reduced fluctuations (compared to the coherent or vacuum state) in one quadrature and increased in the other. They are produced by non-linear interactions, with the parametric down conversion process in a crystal being one of the most commonly used methods (see [38] and references therein). This interaction can be described in terms of the Hamiltonian $\hat{H} = \hbar\chi(\hat{a}^2 - \hat{a}^{\dagger 2})$, and its unitary evolution introduces the so-called *squeezing operator*, given by $\hat{S}(k) = \exp[-\frac{k}{2}(\hat{a}^2 - \hat{a}^{\dagger 2})]$. In this expression, $k = 2i\chi\tau$ is the squeezing parameter, χ the non-linear coupling parameter and τ the interaction time. By applying $\hat{S}(k)$ to a vacuum state $|0\rangle$, we obtain the *squeezed-vacuum* state $|\text{SV}\rangle = \hat{S}(k)|0\rangle$, while the displaced squeezed vacuum state $|\text{DSV}\rangle$ can be obtained by applying the displacement operator $\hat{D}(\alpha)$ on $|\text{SV}\rangle$, i.e. $|\text{DSV}\rangle = \hat{D}(\alpha)\hat{S}(k)|0\rangle$, whose wavefunction in x -representation is $\psi_{\text{DSV}}(x) = \pi^{-1/4} e^{-k/2} \exp[-e^{2k} \frac{(x-x_0)^2}{2} + ipx - i\frac{x_0 p_0}{2}]$. The Wigner function of these states corresponds to a Gaussian which has been ‘squeezed’ along one of its quadratures and stretched in the other. According to the transformation used in equation (2) reads,

$$W_{\text{DSV}}(\beta) = \frac{2}{\pi} e^{-2\left|\frac{(\beta-\alpha)}{e^{-2k}} + \frac{(\beta^*-\alpha^*)}{e^{2k}}\right|^2}. \quad (4)$$

Figure 4 shows an example of a calculated homodyne trace (left panel) and the corresponding Wigner function (right panel) of an amplitude squeezed state with $|\alpha| = 2$ and $k = 0.8$.

2.4.3. CSSs and optical ‘cat’ states. Superpositions of coherent states that differ in amplitude and/or phase can exhibit genuine quantum features without a classical counterpart [37, 106, 107, 118]. The generic form of a CSS in a single field mode is given by $|\text{CSS}\rangle = \sum_i \xi_i |\alpha_i\rangle$, with $\alpha_i \neq \alpha_j \ \forall i \neq j$, and where ξ_i is the corresponding probability amplitude. In the case where the superposition is composed by two coherent states of equal amplitude $|\alpha|$ and opposite phase, the state takes the form $|\text{cat}\rangle_{\pm} = \frac{1}{N_{\pm}} (|\alpha\rangle \pm |-\alpha\rangle)$, where $N_{\pm} = \sqrt{2(1 \pm e^{-2|\alpha|^2})}$ are

the corresponding normalization factors. Because $|\text{cat}\rangle_+$ and $|\text{cat}\rangle_-$, when expanded in the Fock basis, contain only even and odd photon numbers, respectively, are usually referred to as *even* and *odd* optical Schrödinger ‘cat’ states. This is because, within the optical domain, they resemble the quantum superposition of distinguishable classical states envisaged in Schrödinger’s cat *Gedankenexperiment* [119]. This can be directly seen by their wavefunction in x -representation $\psi_{\pm}(x) \propto e^{-(x-x_0)^2/2} \pm e^{-(x+x_0)^2/2}$, which shows two peaks, one at $+x_0$ (which would correspond to a *dead cat*) and one at $-x_0$ (a *live cat*). Also, depending on the amplitude $|\alpha|$ of the coherent states in the superposition, the states are named optical ‘kitten’ and large optical ‘cat’ states for small and large amplitudes, respectively [120]. In a more general case, when the superposition of two coherent states has the form

$$|\text{CSS}\rangle = |\alpha_1\rangle \pm \xi |\alpha_2\rangle, \quad (5)$$

we will refer to it as a *shifted ‘cat’ state*, where $\xi = \langle\alpha_1|\alpha_2\rangle = e^{-\frac{1}{2}(|\alpha_1|^2+|\alpha_2|^2-2\alpha_1^*\alpha_2)}$ is the coupling of the two states. The Wigner function of an optical ‘cat’ state depicts a ring-shaped structure with negative values in the region where the two coherent states overlap. For large optical ‘cat’ states, the Wigner function depicts two pronounced Gaussian-like maxima at $(\pm x_i, \pm p_i)$, where $\pm x_i = \langle\alpha_i|\hat{x}|\alpha_i\rangle$ and $\pm p_i = \langle\alpha_i|\hat{p}|\alpha_i\rangle$, with a strong interference pattern with negative values in the region where the two coherent states overlap. In both cases, the negative values are associated with pure quantum interference effects. Applying the transformation used in equation (2), the Wigner function of equation (5) reads

$$W(\beta) = \frac{2}{\pi N} \left[e^{-2|\beta-\alpha-\chi|^2} + e^{-|\chi|^2} e^{-2|\beta-\alpha|^2} - (e^{2(\beta-\alpha)\chi^*} + e^{2(\beta-\alpha)^*\chi}) e^{-|\chi|^2} e^{-2|\beta-\alpha|^2} \right], \quad (6)$$

where $N = 1 - e^{-|\chi|^2}$ is the normalization factor for $|\text{CSS}\rangle = |\alpha_1\rangle - \xi |\alpha_2\rangle$ with $|\alpha_1\rangle = |\alpha_2 + \chi\rangle$. Figures 5 shows two examples of the calculated homodyne trace (left panels), and the corresponding Wigner functions (right panels) of a shifted optical ‘cat’ and a shifted large optical ‘cat’ state, respectively.

The optical ‘cat’ states are considered as a resource for a vast variety of investigations in quantum technology and QI science. However, their generation is non-trivial and requires the implementation of sophisticated quantum optical protocols. The first observation of the ‘cat’ states was achieved in atoms by the pioneering works of S Haroche and D J Wineland, where the states were created by means of cavity QED and ion trap experiments [14, 15]. Later, and particularly from 2004 to 2017, fully optical methods in quantum state engineering were developed for the generation of optical ‘cat’ and ‘kitten’ states (see [48, 49, 51, 120, 121]). These methods, were developed by means of linear optical elements and the use of Fock, coherent, and squeezed light states as primary sources. However, the low photon number ‘cat’ states delivered by these sources restricts their applicability in many novel investigations in quantum technologies, which can be greatly advanced by the development of new schemes that

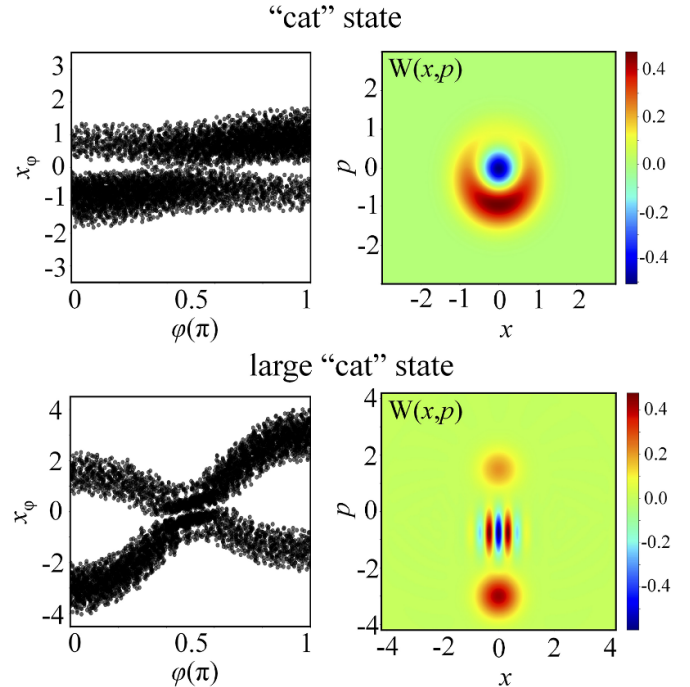


Figure 5. Examples of homodyne traces and Wigner functions of coherent state superpositions $|\text{CSS}\rangle = \xi_1 |\alpha_1\rangle + \xi_2 |\alpha_2\rangle$. The left panels show the calculated homodyne detection signal x_ϕ , and the right panels the corresponding Wigner function $W(x, p)$. (Upper panel): A shifted optical ‘cat’ state with $\xi_1 = 0.7$, $\xi_2 = -1$, $\alpha_1 = 0.3$ and $\alpha_2 = -0.6$. (Lower panel): A shifted large optical ‘cat’ state with $\xi_1 = 0.7$, $\xi_2 = -1$, $\alpha_1 = 1.5$ and $\alpha_2 = -3$.

can lead to the generation of high-photon-number optical ‘cat’ states with controllable quantum features. Such schemes have recently been developed by means of intense laser–matter interactions. Specifically, recent theoretical and experimental investigations [52, 53, 98], conducted using fully quantized approaches in the strong-field limit, have shown that the intense laser–atom interactions and conditioning approaches [99–102] in the process of high-harmonic generation, can be used for the generation of high photon number non-classical and entangled light states with controllable quantum features [53, 98, 103–105]. This matter will be further discussed in section 4.

2.4.4. Entangled states. So far we have only considered a single mode of the electromagnetic field, which can be described by a state $|\psi_1\rangle$, e.g. with a Fock, coherent or squeezed state. However, if we take into account an additional mode of the field, described by the state $|\psi_2\rangle$, we can now consider the total system of the field composite of the two modes. Since we now have two modes, which can, for instance, be different spatial or frequency modes, we can speak about a bipartite system in which each field mode represents one subsystem. The total state of the field, for example, is now given by the tensor product $|\psi_1\rangle|\psi_2\rangle$. However, the most generic case of the total state for the two field modes is expressed in a basis expansion for each mode

$$|\Psi\rangle = \sum_{ij} c_{ij} |i\rangle |j\rangle, \quad (7)$$

where $c_{ij} = \langle ij | \Psi \rangle$ for the basis states $|i\rangle$ and $|j\rangle$ for the two modes, respectively. The state $|\Psi\rangle$ is now said to be entangled, if it can not be written in a separable tensor product form, i.e. $|\Psi\rangle \neq |\psi_1\rangle |\psi_2\rangle$. The fact that the quantum formalism allows for entanglement [122] initially caused interpretational difficulties by means of the famous work from Einstein, Podolsky, Rosen and Schrödinger [119, 123], leading to questions on and study of the foundations of quantum theory [122]. Almost 90 years later, the concept of entanglement has evolved into a versatile tool and resource for modern quantum technologies [124].

For the purpose of this manuscript, we focus on the description of entangled states of different frequency modes of the field, each represented by a coherent state. Such entangled coherent states [125] will be found in the analysis of the process of HHG [98, 102, 103] (see section 4). In addition to using the process of HHG, entangled coherent states can be generated using interferometer schemes [126] or when a coherent state superposition is impinged onto a beam splitter [127].

3. Fundamentals of intense laser-matter interactions: semi-classical approaches

The tremendous progress in fs laser pulse engineering [128–132] has led to the development of table-top laser systems, which nowadays can deliver high power laser pulses of duration down to few optical cycles, and carrier wavelength ranging from the visible and near-infrared (IR), up to mid-IR spectral range [133–136], and THz pulses [137, 138].

The high intensities achievable with these pulses have enabled the investigation of laser-matter interactions in the strong-field limit, where the laser-electric field strength is approaching the binding field inside the atoms themselves. Interactions in this intensity region led to the observation of many fascinating non-linear processes in all states of matter. Among these, is the intense laser-atom interaction and the process of HHG, which has opened the way for numerous investigations ranging from the high-resolution spectroscopy in XUV to AP. A typical scheme used for investigating these interactions is shown in a simplified way in figure 6. Briefly, a linearly polarized fs laser pulse is focused into a target. Considering atoms (noble gases) as a target medium, the intensity of the driving laser pulse in the interaction area is typically $I_L \gtrsim 10^{14} \text{ W cm}^{-2}$. The interaction leads to the generation of ions, photoelectrons, and high-harmonic photons emitted in the propagation direction of the laser field. Due to the non-linearity of the harmonic generation process the divergence of the harmonic beam is smaller than the driving field. Central to these studies is the measurement, and characterization of the interaction products of photons and charges (electrons, ions). Such studies are typically conducted using conventional detectors/spectrometers and pump-probe schemes for measuring ultrafast processes, while the description of the interaction process and the interpretation of the experimental results is based on semi-classical approaches.

Intense laser-atom interaction is one of the most fundamental processes in SLP. For this reason and for introducing the terminology and definitions relevant to the present article, in the next section, we will discuss the fundamentals of this interaction.

3.1. Intense laser-atom interaction

The main features of intense laser-atom interaction can be understood using theoretical tools developed over the past decades, starting with the seminal work by Keldysh in the 1960's [139–143]. According to Keldysh theory, an electron can be freed from an atomic core via multiphoton, tunnel or above-the-barrier ionization. These regimes can be characterized by the Keldysh parameter $\gamma = \sqrt{I_p/(2U_p)}$, where I_p is the ionization potential of the atoms, $U_p(\text{eV}) = F_0^2/(4\omega_L^2) \approx 9.33 \cdot 10^{-14} [I_L(\text{W/cm}^2)\lambda_L^2(\mu\text{m})]$ is the ponderomotive energy, i.e. the average oscillation energy of the electron in a laser field with amplitude F_0 and frequency ω_L . The multiphoton ionization is dominating when $\gamma \gg 1$, while for $\gamma < 1$ and $\gamma \ll 1$ the dominant processes are the tunneling and the above barrier ionization, respectively (figure 7(a)). The majority of the investigations in HHG and attosecond science are performed in experimental conditions where $\gamma \lesssim 1$ and the harmonic emission is phase matched. In the intensity regime where $\gamma \lesssim 1$, the electron tunnels out from the atomic potential bent by the laser field $E(t)$, then accelerates in the laser field from which it gains kinetic energy and then it may recollide elastically or inelastically with the parent ion. The interaction has been successfully described by classical or semi-classical models, namely the three-step model [70–72, 83], treating the electromagnetic field classically. This recollision process is repeated every half-cycle of the driving laser field and leads to the generation of electrons via above-threshold ionization (ATI) and high-order ATI (HATI) processes (figures 7(b) and (c)), high harmonic photons (figure 7(d)) and doubly charged ions via NSDI (figure 7(e)).

3.1.1. ATI and HATI. The first strong-field effect that was conclusively demonstrated in experiment is ATI, i.e. the ionization of a photoelectron through the absorption of more photons than it requires to overcome the ionization barrier. This can range from the so-called 'multiphoton' regime at relatively low fields, where photon-absorption pictures can provide good models, to higher fields where perturbation theory completely breaks down, and quasi-static pictures (typically known as optical tunneling) provide a better description. One of the defining features of ATI is a 'comb' in the photoelectron energy spectrum, where each peak is separated by one photon in energy, and which arises in the time domain as the interference of a sequence of photoelectron wavepackets produced with the periodicity of the driving laser.

The earliest observations of ATI [144] required only a few photons, and could still be explained within LOPT. However, later results [145] demonstrated a clear breakdown

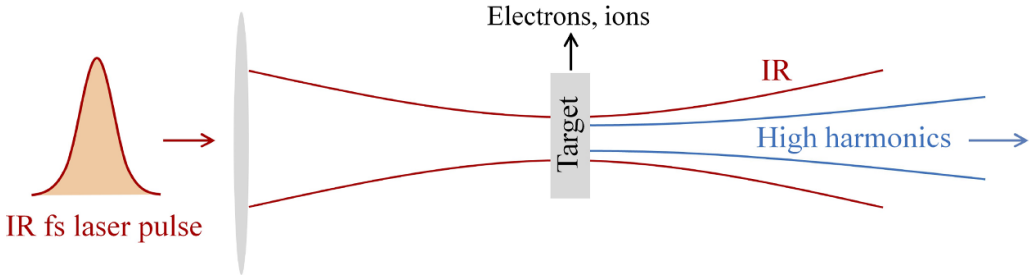


Figure 6. A sketch of a typical approach used for investigating intense laser–matter interactions. An IR laser pulse is focused into a target area which contains the medium to be investigated (atoms, molecules, solids, etc). Considering atoms as a target medium, the intensity of the driving laser pulse in the interaction area is typically $I_L \gtrsim 10^{14} \text{ W cm}^{-2}$ for noble gases. The medium length is smaller than the confocal parameter of the driving laser and thus experiences the same intensity along the propagation direction. The interaction products are electrons, ions and high harmonics emitted in the direction of the driving field.

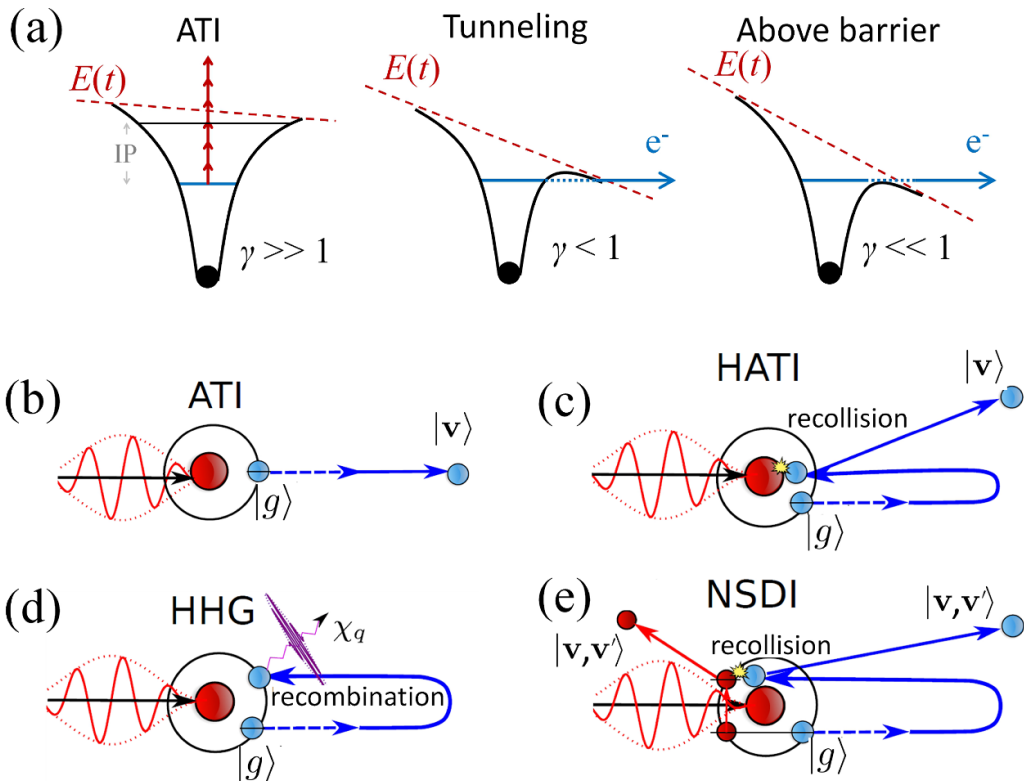


Figure 7. (a) A drawing of intense laser–atom interaction. An IR laser pulse is focused into a target area which contains atoms (typically noble gases). The intensity of the laser pulse in the interaction area is typically $I_L \gtrsim 10^{14} \text{ W cm}^{-2}$. The atomic Coulomb potentials under the influence of the laser field $E(t)$ are shown for ATI, tunnel ionization, and above-barrier ionization cases. The multiphoton absorption is depicted by red vertical arrows. IP is the ionization potential and γ is the Keldysh parameter. The electron tunnels out from the atomic potential bent by the laser field, then accelerates in the laser field from which it gains kinetic energy and then it may recollide elastically or inelastically with the parent ion. The process is repeated every half-cycle of the driving laser field and leads to the generation of electrons (via ATI and HATI processes), ions (via NSDI) and high harmonic photons. (b)–(e) Schematics of HHG, ATI, HATI and NSDI processes. The initial and final electronic states are given by $|g\rangle$ and $|\mathbf{v}\rangle$, respectively. Two classical light fields are depicted, in red is the incident intense IR laser field, while the harmonic emission is in purple. It is noted that the electron trajectories are along the polarization of the driving laser field (not shown in the graphs).

of perturbation theory, leading to the application of tunneling theories such Keldysh-Faisal-Reiss theory [139, 141, 146] and, eventually, to the development of the widely applied strong-field approximation (SFA) [147, 148] and its semi-classical interpretation, which linked to the classical picture, the three-step model [70, 71]. For a complete review on the history and the current status of the SFA, see [83]; see also

[149] for a wider review of the theoretical methods of attoscience and strong-field physics.

The three-step model for ATI provides a clear physical picture of the process, separated into two components: (i) direct ATI, shown in figure 7(b), where an electron is released from a target via a strong laser field and propagates to the detector driven predominantly by the laser field and without significant

further interactions with its parent ion, and (ii) HATI, shown in figure 7(c), where the ionized electron undergoes a laser-driven elastic recollision with its parent. The direct ATI process is associated with a relatively low photoelectron energy, with a classical cutoff of $2U_p$. In contrast, the HATI process is associated with a much higher photoelectron energy, and it is typically present as a long plateau with a cutoff at $10U_p$ [150], which directly mimics the classical dynamics of the three-step model. However, the recollision dynamics is generally much richer—and much more quantum mechanical—than the three-step model, and indeed the returning electron comes back as a high-energy wavepacket with a very short wavelength which can be used, among other things, to form images of the parent atomic or molecular ion, as is the case in laser-induced electron diffraction [151, 152], as discussed below, or in photoelectron holography [153, 154].

3.1.2. HHG. The recollision process in HATI between the tunneled photoelectron and its parent ion is one of the core dynamical features of strong-field physics, because—in addition to the elastic scattering in HATI—it can lead to a variety of outcomes, including inelastic scattering and further ionization of the parent. Most notably, it can also lead to the recombination of the photoelectron (which carries significant kinetic energy) back into the electronic hole it left in the parent. That recombination results in the emission of a high-frequency burst of radiation, in the form of a sharp pulse of light that is typically as short as a few tens of attoseconds. These pulses normally form a periodic train of pulses whose frequency spectrum forms harmonics of the laser driver, which prompts this emission to be named HHG (figure 7(d)).

Informally, this emission is typically thought of as the emission of a single photon that carries away the kinetic energy of the photoelectron. One of the key goals of this work is to elucidate the degree to which this photon picture has a rigorous matching theoretical description within the QO realm. The emitted radiation, similarly to the photoelectron in HATI, normally forms a harmonic frequency comb with a long and flat plateau which terminates at a sharp cutoff that gives way to an exponential decay of the emission. The location of this cutoff is governed by the so-called ‘cutoff law’ [72, 83, 155], $\hbar\Omega_{\text{cutoff}} = 3.17U_p + 1.32I_p$, which includes the classical three-step model’s prediction [70, 71] that the maximal recollision energy of the electron is $3.17U_p$, with the addition of the binding energy I_p , which is suitably amended by a quantum correction factor of 1.32 [72, 155].

Experimentally, HHG was first observed at the end of the 1980s [73, 156], and quickly developed into an attractive light source of attosecond pulses based on the realization that the emitted harmonics are phase-locked [157]. As the subject has matured, both the microscopic [158] and macroscopic phase-matching [159–162] aspects of HHG have come into sharper control, allowing the subject to expand into a wide variety of directions, from studies of the conservation laws of the HHG emission when seen as a parametric nonlinear optical process [163–169] to multicolor tailoring of the waveform

to optimize the harmonic cutoff [170–172], detailed tailoring of the polarization state of the harmonic emission [165, 166, 173], the harnessing of resonances in the continuum states of the target [149, 174–176], and the control over optical singularities in the emitted beam [167–169, 177], among many others.

3.1.3. Non-sequential double ionization (NSDI). The above processes, HATI and HHG, elucidate the cases where a laser-driven recollision leads to an elastic recollision or recombination, respectively. However, if the recolliding photoelectron undergoes an inelastic recollision this may lead to further ionization via NSDI or non-sequential multiple ionization (NSMI). The first evidence for NSDI and NSMI was found in [178], where ionization yields of multiply ionized targets did not match the predictions corresponding to a sequential ionization mechanism. The change in ionization rate from the non-sequential regime to the sequential regime, as laser intensity is increased, gave rise to the famous knee structure [179]. This non-sequential behaviour was ultimately attributed to a recollision mechanism [180, 181], described as a three-step mechanism [71], in direct analogy with HHG and HATI. The semi-classical processes associated with NSDI is depicted in figure 7(e). One of the strongest indicators of recollision in NSDI was the high correlation between the two electrons [181]. Recently, it has been shown in some cases, specifically for lower laser intensities, the orbital angular momentum (OAM) of the two photoelectrons is entangled [182].

3.1.4. The strong field approximation. Strictly speaking, the interaction of matter with intense laser fields is described by the time-dependent Schrödinger equation (TDSE) that captures both the evolution of the wave functions and the time evolution of the physical observables. However, the solution of the TDSE in all the degrees of freedom of the system is computationally very demanding. Moreover, a physical interpretation of the numerical results is highly nontrivial. Considering this, approximate methods are more than welcome. Such a method is the SFA [72], which has consistently been shown over the years to be the workhorse tool for describing intense laser-matter interactions. Because the method has been extensively studied and reported over the years (see [83]), here, we will mention only the very fundamentals in case of intense laser atom interactions.

The non-relativistic TDSE of an atom interacting with a single-mode long-wavelength (IR) linearly-polarized laser field $\mathbf{E}_{\text{cl}}(t)$ of frequency ω_L reads,

$$i\hbar \frac{\partial |\Psi(t)\rangle}{\partial t} = \hat{H}|\Psi(t)\rangle, \quad (8)$$

where the Hamiltonian, $\hat{H} = \hat{H}_a + \hat{H}_{\text{int}}$, describes the laser-target system in the single-active-electron (SAE) approximation. Here, \hat{H}_a is the atomic Hamiltonian and $\hat{H}_{\text{int}} = e\mathbf{E}_{\text{cl}}(t) \cdot \hat{\mathbf{r}}$ is the interacting Hamiltonian under the dipole approximation which describes the coupling of the atom, via the dipole operator $\hat{\mathbf{d}} = e\hat{\mathbf{r}}$, to a classical field $\mathbf{E}_{\text{cl}}(t)$.

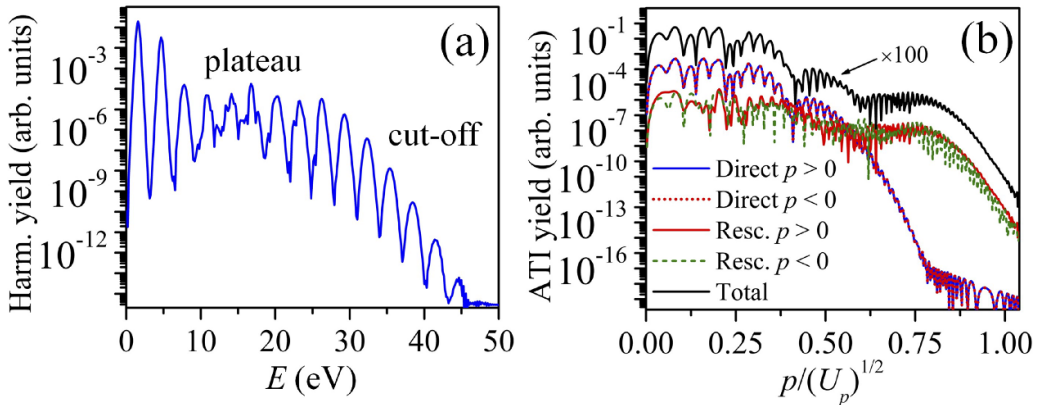


Figure 8. HHG (a) and ATI (b) spectra calculated when Xenon atoms interact with a linearly polarized laser pulse of intensity $8 \times 10^{13} \text{ W cm}^{-2}$ and $\sim 30 \text{ fs}$ duration. In (b) the photoelectron spectrum corresponding to direct, rescattered photoelectrons with positive ($p > 0$) and negative ($p < 0$) momenta are shown with different colors. The ATI spectrum shown with black solid curve, which includes the contribution of the direct and rescattered electrons, has been shifted by a factor of 100 for visualization reasons. Reproduced from [98]. CC BY 4.0.

In the region of $\gamma < 1$, the effects of atomic effective potential on the dynamics of electrons in the continuum are assumed to be small, and they can be treated using perturbation theory. This suggests the following formulation of the ‘standard SFA’: (i) The strong laser field does not couple with any bound state beyond the ground state, which we represent by $|g\rangle$, so that together with the continuum (scattering) states, $|\mathbf{v}\rangle$ (where \mathbf{v} is the momentum of the electron in the continuum), are the states involved in the dynamics. (ii) The amplitude of the ground state is considered to be ≈ 1 , i.e. the ground state of the atom is not depleted. (iii) In the continuum, the electronic states are taken from the basis of exact scattering states, which are eigenstates of $\hat{H}_a|\mathbf{v}\rangle = \frac{\mathbf{v}^2}{2m}|\mathbf{v}\rangle$ with fixed momentum \mathbf{v} . However, the dominance of the strong laser field allows the perturbative expansion of the continuum states about the binding field, where to zeroth order, the electron can be considered as a free particle moving in the laser field without the influence of the atomic potential. After making these approximations, the wave function can be written as $|\Psi(t)\rangle = e^{i\hat{p}_t t}(|g\rangle + \int d^3\mathbf{v} b(\mathbf{v}, t)|\mathbf{v}\rangle)$ and the TDSE, equation (8), can be solved exactly with the $b(\mathbf{v}, t)$ to be in a closed form. Thus, the ion, electron and HHG spectra can be calculated (using the saddle point method) by the ionization amplitudes $b(\mathbf{v}, t)$ and the dipole matrix element $\langle\Psi(t)|\hat{\mathbf{r}}|\Psi(t)\rangle$, respectively. Figure 8 shows a representative example of the HHG and ATI spectra that have been calculated (using the QPROP software [183]) when Xenon atoms interact with a linearly polarized laser pulse of intensity $8 \times 10^{13} \text{ W cm}^{-2}$ and $\sim 30 \text{ fs}$ duration.

4. Intense laser–atom interaction: fully quantized approach

The fully quantized description of intense laser–atom interaction and the conditioning approach that has been used for the generation of non-classical and entangled states has been extensively discussed in recent publications [52, 53, 98, 103, 105]. Here, we summarize the main findings, emphasizing the results associated with potential applications in QI science.

The fully quantized description of intense laser–atom interaction is shown schematically in figure 9, where $|\alpha_L\rangle$ and $|\alpha_L + \chi_L\rangle$ are the states of the driving field mode before and after interaction, respectively. $|\chi_q\rangle$ are the states of the generated high-order harmonic modes, and $|g\rangle$ and $|\mathbf{v}\rangle$ are the initial and final electronic states, respectively. It is noted that the electrons in NSDI may be entangled [182], and therefore are written as a two-particle state. The quantum optical degrees of freedom may also be entangled with each other and the electronic states, however, for clearer labelling we have written these separately.

4.1. QED of intense laser–atom interactions

We start by considering a situation where only a single electron of the atom participates in the dynamics, and is initially in the ground state of the system, which we denote by $|g\rangle$. We characterize the laser field with a coherent state of amplitude α_L , populating the mode of frequency $\omega_L \in \text{IR}$, while all the other modes remain in a vacuum state, i.e. $|\Phi_i\rangle = |\alpha\rangle \otimes_{q=2}^{N_c} |0_q\rangle$. For the sake of simplicity, we consider a discrete set of modes of frequency $\omega_q = q\omega_L$, $q \in \mathbb{N}$ and introduce a cutoff frequency $N_c\omega_L$, beyond which no harmonics are considered. We set this frequency to be higher or equal to the cutoff frequency of the HHG spectrum. With all the above, we can write the initial state of the system prior to the dynamics as $|\Psi(t_0)\rangle = |g\rangle \otimes |\alpha_L\rangle \otimes_{q=2}^{N_c} |0_q\rangle$.

The Hamiltonian characterizing the dynamics between the laser and a single electron of the corresponding atom, is given by $\hat{H} = \hat{H}_a + \hat{H}_f + \hat{H}_{\text{int}}$, where \hat{H}_a is the atomic Hamiltonian, \hat{H}_f is the Hamiltonian of the electromagnetic field (as given in section 2.1), and \hat{H}_{int} describes the interaction between light and matter. Under the length-gauge and dipole approximation, the latter can be written as $\hat{H}_{\text{int}} = \hat{\mathbf{d}} \cdot \hat{\mathbf{E}}$, with $\hat{\mathbf{d}}$ the dipole moment operator and $\hat{\mathbf{E}} = i\mathbf{g}(\omega_L) \sum_{q=1}^{N_c} (\hat{a}_q - \hat{a}_q^\dagger)$ the electric field operator. In order to simplify the description of these dynamics, we move to a more convenient frame by applying a set of unitary transformations, whose effect on the quantum optical state in phase space is pictorially presented in figure 10.

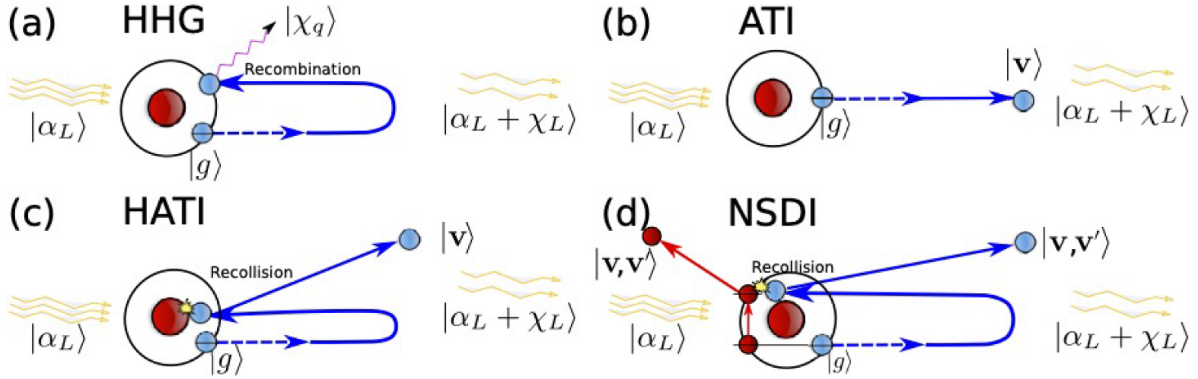


Figure 9. A schematic of the fully quantized description of intense laser–atoms interaction. From (a) to (d), the HHG, ATI, HATI and NSDI. Reproduced from [98]. CC BY 4.0.

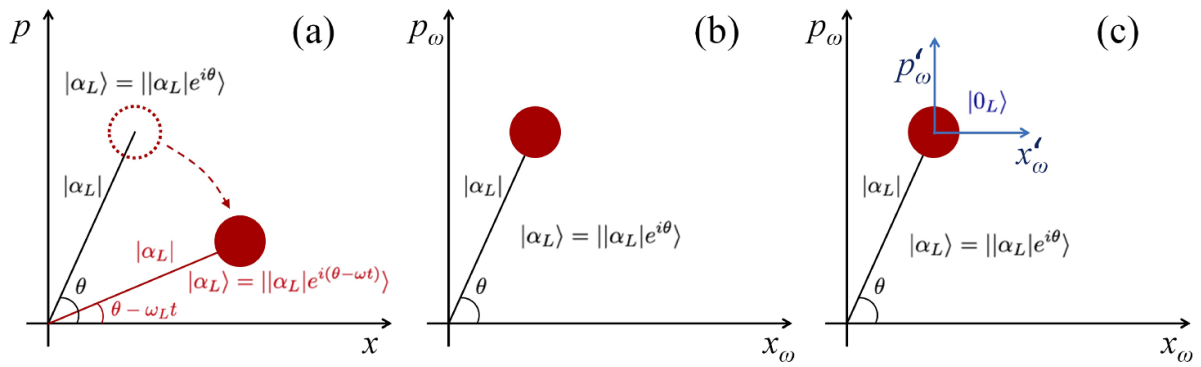


Figure 10. Pictorial representation showing how the unitary transformations affect our frame of reference in the quantum optical phase space. (a) Initially, if no transformations are applied and we consider only the dynamics due to H_f , the coherent state of the field rotates with frequency ω_L around the phase space origin. (b) When we work in the interaction picture with respect to H_f , our frame of reference oscillates with frequency ω_L , since the time-dependence due to this Hamiltonian goes to the operators, and the quantum optical state gets fixed in the phase space. (c) Finally, we perform a translation of our frame of reference, such that its origin is now located on top of the coherent state. Thus, in this new frame, the coherent state is given in terms of the vacuum state $|0_L\rangle$.

First, we move to the interaction picture with respect to H_f , which makes our frame of reference to rotate with the frequency of the field (see figure 10(b)), and therefore introduces a time-dependence in the electric field operator, i.e. $\hat{\mathbf{E}} \rightarrow \hat{\mathbf{E}}(t)$ with $\hat{a}_q \rightarrow \hat{a}_q e^{-i\omega_q t}$. Second, we displace our frame of reference in phase-space by α_L , such that the initial IR coherent state $|\alpha_L\rangle$ is in the origin of the shifted frame. To account for this shift in the Hamiltonian, the electric field splits into two components, i.e. $\hat{\mathbf{E}}(t) \rightarrow \mathbf{E}_{cl}(t) + \hat{\mathbf{E}}(t)$, where the first is the mean value of the electric field in the initial state $|\Phi_i(t_0)\rangle = |\alpha_L\rangle \otimes_{q=1}^{N_c} |0_q\rangle$, i.e. $\mathbf{E}_{cl}(t) = \text{Tr}[\hat{\mathbf{E}}(t)|\Phi_i(t_0)\rangle\langle\Phi_i(t_0)|]$, and the second term provides the quantum fluctuations around the mean value. Finally, we work in the interaction picture with respect to the semiclassical Hamiltonian $\hat{H}_{sc}(t) = \hat{H}_a + \hat{\mathbf{d}} \cdot \mathbf{E}_{cl}(t)$, which makes the dipole operator time-dependent, i.e. $\hat{\mathbf{d}} \rightarrow \hat{\mathbf{d}}(t)$. With this last transformation, we encapsulate all the dynamics found in the semiclassical analysis [72, 83], into the time-dependent dipole operator, and we are thus left with a Hamiltonian $\hat{H}'(t) = \hat{\mathbf{d}}(t) \cdot \hat{\mathbf{E}}(t)$ coupling the electron dipole moment to the electric field operator. The corresponding Schrödinger equation is given by

$$i\hbar \frac{d|\psi(t)\rangle}{dt} = \hat{\mathbf{d}}(t) \cdot \hat{\mathbf{E}}(t) |\psi(t)\rangle, \quad (9)$$

and the initial condition is now given by $|\psi(t_0)\rangle = |g\rangle \otimes_{q=1}^{N_c} |0_q\rangle$, where $q=1$ corresponds to the driving IR frequency. This differential equation, constitutes the basis of the upcoming analysis.

4.1.1. Conditioning on HHG using single-color driving fields: generation of optical ‘cat’ and entangled states from XUV to IR. In order to characterize the quantum optical state after the HHG processes, where the electron is found on its ground state, we project equation (9) onto $|g\rangle$, and denote the state of light as $|\Phi(t)\rangle = \langle g|\psi(t)\rangle$. We further introduce the SFA version of the identity, $1 = |g\rangle\langle g| + \int d\mathbf{v}|\mathbf{v}\rangle\langle\mathbf{v}|$, where the contribution of the excited bound states have been neglected since they barely participate in the dynamics, in virtue of the strong-field approximations [72]. However, further neglecting the contribution of the electronic continuum states $|\mathbf{v}\rangle$, since the continuum amplitude is much smaller than the ground state amplitude, we get that the dynamics of $|\Phi(t)\rangle$ can be described by

$$i\hbar \frac{d|\Phi(t)\rangle}{dt} = \langle \mathbf{d}(t) \cdot \hat{\mathbf{E}}(t) | \Phi(t) \rangle, \quad (10)$$

where $\langle \mathbf{d}(t) \rangle = \langle g | \hat{\mathbf{d}}(t) | g \rangle$ is the time-dependent expectation value of the dipole moment with respect to the ground state.

Since the commutator of the new interaction Hamiltonian in (10) at different times is just a complex number, the different field modes will not couple when solving the Schrödinger equation in (10). Thus, each of the field modes undergoes an independent evolution, and a *classical* oscillating current is coupled to each of the modes. As discussed in section 2.2, the unitary evolution corresponding to a Hamiltonian of this form can be written in terms of the displacement operator, inducing a shift in the phase-space of the corresponding quantum optical mode. Hence, we find that the quantum optical state of the system after these dynamics is given by

$$|\Phi(t)\rangle = e^{i\varphi(t,t_0)} \bigotimes_{q=1}^{N_c} \hat{D}(\chi_q(t,t_0)) |0_q\rangle. \quad (11)$$

As an output, we get a coherent displacement in the quantum optical field modes of a quantity $\chi_q(t,t_0)$, given by

$$\chi_q(t,t_0) = -\frac{1}{\hbar} \int_{t_0}^t dt' \mathbf{g}(\omega_L) \cdot \langle \mathbf{d}(t') \rangle e^{i\omega_q t}, \quad (12)$$

which corresponds to the Fourier transform of the time-dependent dipole moment. The absolute value of this quantity, when considering the limit $t \rightarrow \infty$, leads to the known features of the HHG spectrum [98]. The approximation leading to (10) has the underlying assumption of vanishing correlations in the dipole moment operator [102, 184]. We note that, so far, we have been working under single-atom dynamics, and therefore the generated shift $\chi_q(t,t_0)$ is very small. Nevertheless, this solution can be extended to a more realistic scenario, where we have N_{ph} atoms participating in the dynamics in a phase-matched way, by multiplying the shift with the number of phase-matched atoms N_{ph} , i.e.

$$\chi_q(t,t_0) \rightarrow N_{ph} \chi_q(t,t_0). \quad (13)$$

The solution we have obtained in equation (11) is given by the tensor product of the coherent states $\{|\chi_q(t,t_0)\rangle\}_{q=1}^{N_c}$, and is therefore what we referred to in section 2 as a *classical* state. Nevertheless, by introducing conditioning measurements on the harmonic field modes, we could potentially generate non-classical states of light in the form of coherent state superpositions and entangled coherent states between different frequency modes. Such conditioning operations are possible because, as a consequence of the light–matter interaction, each of the field modes gets excited from the same dipole moment, making the respective shifts $\chi_q(t,t_0)$ correlated. Thus, the mode that is actually excited during the HHG process is a wavepacket mode taking into account these correlations [52, 98, 102, 103], and that can be described with a set of number states $\{|\tilde{n}\rangle\}$. Here, the state $|0\rangle$ describes the case where no harmonic radiation is generated, and therefore corresponds to the initial quantum optical state. On the contrary, $|\tilde{n}\rangle$ with $\tilde{n} \neq 0$, describes the case where harmonic radiation has been generated. This allows us to define a set of

positive operators $\{\Pi_{\tilde{0}}, \Pi_{\tilde{n} \neq \tilde{0}}\}$, describing whether harmonic radiation is generated or not, or equivalently whether the wavepacket which takes into account the correlations between the field modes has been excited or not. Specifically, the element $\Pi_{\tilde{0}} = |\tilde{0}\rangle\langle\tilde{0}|$ projects onto the subspace where no excitations are found, while $\Pi_{\tilde{n} \neq \tilde{0}} = \sum_{\tilde{n} \neq 0} |\tilde{n}\rangle\langle\tilde{n}| = 1 - |\tilde{0}\rangle\langle\tilde{0}|$ onto the subspace where HHG excitations are found. The *conditioning on HHG* operation corresponds to this second case, and can be witnessed by the detection of harmonic radiation. Applying this operation onto the state given in equation (11) leads to

$$|\Phi_{\text{HHG}}(t)\rangle = |\alpha_L + \chi_1(t,t_0)\rangle \bigotimes_{q=2}^{N_c} |\chi_q(t,t_0)\rangle - \xi_1(t,t_0) |\alpha_L\rangle \bigotimes_{q=2}^{N_c} \xi_q(t,t_0) |0_q\rangle, \quad (14)$$

where in this expression we have undone the displacement transformation $\hat{D}(\alpha_L)$ introduced in order to arrive to equation (9), and we have defined $\xi_1(t,t_0) = \langle \alpha | \alpha + \chi_L(t,t_0) \rangle$ and $\xi_q(t,t_0) = \langle 0 | \chi_q(t,t_0) \rangle$.

The state presented in (14) is a massively entangled state between the field modes. We highlight this as *massive* because the number of modes excited after HHG processes can easily surpass the limit $N_c > 10$. However, the entanglement properties of this state crucially depend on how big are the shifts $\chi_q(t,t_0)$ [103] (see figure 11(a)). Specifically, when these become too large, the quantities $\xi_q(t,t_0)$ become very small and the obtained state becomes separable. This can be seen from equation (14) when considering the limit $\xi_q(t,t_0) \rightarrow 0$, which leads to a separable state of the form $|\Phi_{\text{HHG}}(t)\rangle = |\alpha_L + \chi_1(t,t_0)\rangle \bigotimes_{q=2}^{N_c} |\chi_q(t,t_0)\rangle$. We note that the values of the shifts depend on the harmonic yield, and can be increased or decreased by, for instance, enlarging or reducing the number of atoms participating in the HHG process by varying the gas density [53].

As mentioned before, this scheme can be used for generating coherent state superpositions in the driving field, leading to high-photon number non-classical states of light. Specifically, projecting the state in equation (14) onto the state in which the harmonics are found, i.e. $\bigotimes_{q=2}^{N_c} |\chi_q(t,t_0)\rangle$, we get

$$|\Phi_{\text{HHG}}^{(\text{IR})}(t)\rangle = |\alpha_L + \chi_1(t,t_0)\rangle - \xi_1(t,t_0) |\xi_{\text{HH}}(t,t_0)|^2 |\alpha_L\rangle, \quad (15)$$

where $\xi_{\text{HH}}(t,t_0) = \prod_{q=2}^{N_c} \xi_q(t,t_0)$. The value of $\chi_1(t,t_0)$ determines the distinguishability of the coherent states in the superposition, and therefore leads to the generation of ‘kitten-like’ or ‘cat-like’ states, as shown in figures 11(b) and (c). On the other hand, when $\chi_1(t,t_0)$ becomes excessively large, the second term in the superposition shown in (15) vanishes, and we are left with the coherent state $|\alpha_L + \chi_1(t,t_0)\rangle$. Note that we can equivalently perform the same operations onto an XUV mode, that is, to measure all the field modes (including the fundamental), except one of the harmonic ones. This allows us to obtain coherent state superpositions for frequencies belonging to the XUV region [103], which are given for the mode with frequency $\omega_q = q\omega_L$ by

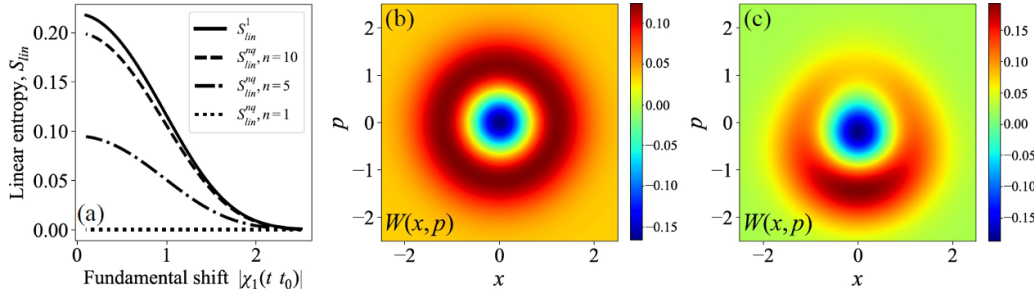


Figure 11. In (a) we show the behavior of the linear entropy as a function of the shift in the fundamental mode. The linear entropy is defined as $S_{\text{lin}}(\rho) = 1 - \text{Tr}(\rho^2)$, where ρ is the partial trace of the entangled state in equation (14) with respect to some of the harmonic modes. This quantity can be used as a measure of entanglement between coherent states [185, 186]. Specifically, S_{lin}^1 (solid curve) shows the entanglement between the fundamental mode and all the other harmonic modes, and S_{lin}^{nq} shows the entanglement between n harmonic modes and the rest (among which we include the fundamental). Reprinted (figure) with permission from [103], Copyright (2022) by the American Physical Society. (b) and (c) show the calculated Wigner functions of the quantum state presented in equation (15) for two different shifts, namely $|\chi_1(t, t_0)| = 0.01$ and $|\chi_1(t, t_0)| = 0.5$, respectively.

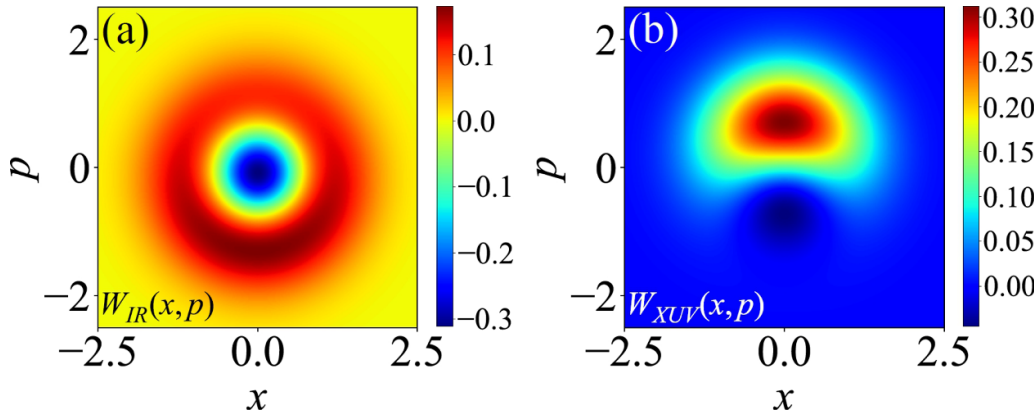


Figure 12. (a) and (b) show the calculated Wigner functions corresponding to a coherent state superposition of the fundamental mode (typically of wavelength $\lambda_{\text{IR}} = 800$ nm), and a coherent state superposition for the q th harmonic mode, respectively. For the calculation, the harmonic cutoff has been set to the 11th harmonic (corresponding to a wavelength of $\lambda_{\text{XUV}} = 72.7$ nm), $\chi_1 = -0.2$, such that $\chi_q \approx 0.03$. The opposite shift in the imaginary part reflects the correlation between the field modes. Reprinted (figure) with permission from [103], Copyright (2022) by the American Physical Society.

$$|\Phi_{\text{HHG}}^{(q)}(t)\rangle = |\chi_q(t, t_0)\rangle - \xi_q(t, t_0)|\bar{\xi}(q, t, t_0)|^2|0\rangle, \quad (16)$$

where we have defined $\bar{\xi}(q, t, t_0) = \prod_{q' \neq q} \xi_{q'}(t, t_0)$. In figure 12 we show an example of the Wigner functions obtained for equations (15) and (16). The opposite shift in phase space reflects the correlation between the field modes [103].

4.1.2. Conditioning on HHG using two-color driving fields: generation of optical ‘cat’ and entanglement between the driving field modes. Using this conditioning technique, together with more elaborated HHG schemes, one can generate a large number of entangled states using frequencies belonging to the visible and IR range. For instance, we can excite the atom by using a two-color driving field, as shown in [103]. In these experiments [165, 187, 188], two-color laser fields of frequencies ω_1 and ω_2 , belonging to the far-IR and visible spectral regions, that have either parallel or orthogonal polarizations, are combined to drive the atomic system. In this case, the initial state of the field is $|\alpha_{\omega_1}\rangle|\alpha_{\omega_2}\rangle$, while the field state after the

HHG process is $|\alpha_{\omega_1} + \chi_{\omega_1}\rangle|\alpha_{\omega_2} + \chi_{\omega_2}\rangle \bigotimes_q^{N_c} |\chi_q\rangle$. After performing the *conditioning on HHG* operation [103], the final quantum optical state can be written as

$$|\Phi_{\text{HHG}}^{(\omega_1 - \omega_2)}(t)\rangle = |\alpha_{\omega_1} + \chi_{\omega_1}\rangle|\alpha_{\omega_2} + \chi_{\omega_2}\rangle - \xi_{(\omega_1, \omega_2)}|\alpha_{\omega_1}\rangle|\alpha_{\omega_2}\rangle, \quad (17)$$

where $\chi_{\omega_1}, \chi_{\omega_2}$ is the depletion of the two-color driving field modes. The factor $\xi_{(\omega_1, \omega_2)}$, is a complex number that depends on the phase and amplitude of the initial coherent states and of the generated shifts.

4.1.3. Conditioning on ATI and generation of optical ‘cat’ states. In ATI processes, the electron is found in the continuum after the end of the pulse (see figure 7). Therefore, with the aim of characterizing the quantum optical state after ATI processes, we project the TDSE in equation (9) with respect to a continuum state $|\mathbf{v}\rangle$. When doing so, and after introducing the SFA version of the identity, we find that considering only direct ATI events, i.e. at zeroth order level with respect to the rescattering matrix elements, we can write the TDSE as [98]

$$i\hbar \frac{d|\Phi(\mathbf{v},t)\rangle t}{dt} = \hat{\mathbf{E}}(t) \cdot \langle \mathbf{v} | \hat{\mathbf{d}}(t) | g \rangle |\Phi(t)\rangle + \hat{\mathbf{E}}(t) \cdot \Delta \mathbf{r} |\Phi(\mathbf{v},t)\rangle, \quad (18)$$

where we have defined $|\Phi(\mathbf{v},t)\rangle = \langle \mathbf{v} | \psi(t) \rangle$, and where $\Delta \mathbf{r}(\mathbf{v},t)$ is the total displacement performed by the electron during its propagation in the continuum, which is given by

$$\Delta \mathbf{r}(t, \mathbf{v}) = \frac{e}{m} \int_{t_0}^t dt' \left[m \mathbf{v} - \frac{e}{c} \mathbf{A}(t) + \frac{e}{c} \mathbf{A}(t') \right], \quad (19)$$

with $\mathbf{A}(t)$ the classical vector potential, defined as $\mathbf{E}_{cl}(t) = -\partial \mathbf{A}(t)/\partial t$.

The differential equation presented in (18), is composed by two terms. The first, introduces the transition matrix element between the ground state and the continuum state, which characterizes the backaction of the ionization process over the field modes. On the other hand, the second term depends on the electronic displacement $\Delta \mathbf{r}(\mathbf{v},t)$, and therefore takes into account the backaction of the electronic motion in the continuum over the field modes. A solution to this differential equation, having in mind that the electron is initially found in the ground state, can be written as [98]

$$|\Phi(\mathbf{v},t)\rangle = -\frac{i}{\hbar} \int_{t_0}^t dt' e^{i\varphi(t,t',\mathbf{v})} \prod_q \hat{D}(\delta_q(t,t',\mathbf{v})) \hat{\mathbf{E}}(t') \cdot \langle \mathbf{v} | \hat{\mathbf{d}}(t') | g \rangle |\Phi(t')\rangle, \quad (20)$$

where $|\Phi(t')\rangle$ is given as in equation (11), and we have defined

$$\delta_q(t,t',\mathbf{v}) = -\frac{1}{\hbar} \int_{t'}^t d\tau \mathbf{g}(\omega_q) \cdot \Delta \mathbf{r}(\tau, \mathbf{v}) e^{i\omega_q \tau}, \quad (21)$$

which is the Fourier transform of the electron's displacement. Thus, from the evolution given by equation (20), we see that the quantum optical state of the system gets displaced first by a quantity $\chi_q(t,t_0)$, as a consequence of the electronic oscillation in the ground state [189], leading to $|\Phi(t')\rangle$. At time t' an ionization process takes place, which is highlighted in the analytical expression by the presence of the transition matrix element $\langle \mathbf{v} | \hat{\mathbf{d}}(t) | g \rangle$, where the electron gets promoted from the initial ground $|g\rangle$ to a continuum state $|\mathbf{v}\rangle$. This event, induces a change on the final state of the field happening at t' , and that is due to the coupling of this matrix element to the electric field operator. Finally, the electron propagates in the continuum driven by the field, as an oscillating and drifting charge, and therefore behaves as a classical charge current. This leads to a shift in the quantum optical state of the field given by $\delta_q(t,t',\mathbf{v})$ for the q th mode, and that depends on the final momentum \mathbf{v} with which the electron is found. We note that these dynamics are for the case of direct ionization, with a kinetic energy of less than $2U_p$. However, the electron can still undergo rescattering processes, which define the high-energy part of the photoelectron spectrum (see section 3.1.1). These extra dynamics, where the electrons can end up with values of the kinetic energy up to $10U_p$, get reflected on the final quantum optical state by an extra coupling to the electromagnetic field

happening when the rescattering takes place (see [98] for more details).

One of the striking features of the quantum optical state after ATI in equation (20), is that the displacement obtained over the field modes, depends on the ionization time t' of the electron, which naturally leads to a quantum superposition. This contrasts with what was found in HHG, where the final state of the system was given as a tensor product between different coherent states, and the superposition was generated by introducing the *conditioning on HHG* operation. Furthermore, the quantum superpositions obtained for ATI, also depend on the final momentum of the electron \mathbf{v} . In this direction, it was found in [98] that the displacement $\delta(t,t',\mathbf{v})$, differed for positive and negative values of the momentum. Specifically, while showing a phase difference of π , the imaginary component of $\delta(t,t',\mathbf{v})$ has opposite signs for positive and negative momentum [98, 105]. This is related to the fact that the sign of \mathbf{v} determines the direction along which the electron is propagating, and therefore determines whether the generated displacement interferes in- or out-of-phase with the input driving field. This leads to either an enhancement or depletion of the fundamental mode, which can be observed by computing the photon number probability distribution $P(n)$, for $|\Phi^{IR}(\mathbf{v},t)\rangle = \langle 0_{HH} | \Phi(\mathbf{v},t) \rangle$, with $|0_{HH}\rangle$ a shorthand notation for $\bigotimes_{q>2} |0_q\rangle$. Here, we have assumed that the harmonic modes remain in the vacuum state $|0_q\rangle$, in order to account for the case where no harmonics are emitted [98]. In figures 13(a) and (b), we show $P(n)$ for two values of \mathbf{v} that are equal in magnitude, but differ in sign. For representation purposes, the initial coherent state has been set to $|\alpha| = 7$, such that the vertical dashed line represents the initial mean photon number. We observe that, for positive momentum (figure 13(a)), the shift tends to enhance the mean photon number, while for negative momentum (figure 13(b)), it tends to lower it. Nevertheless, the influence of positive and negative momentum depends on the carrier-envelope phase, i.e. the phase difference between the envelope and the carrier wave of the pulse, such that a modification in π of this phase, leads to the contrary effect. On the other hand, the double peak structure in both plots witness the fact that the final state is given as superposition between coherent states [98, 105].

This difference on the final quantum optical state of the field for positive and negative momentum, could be used for the generation of entangled states between light and matter [105]. In particular, when restricting to ATI processes, the total state of the system can be written as

$$|\psi(t)\rangle = \int d\mathbf{v} |\mathbf{v}\rangle |\Phi(\mathbf{v},t)\rangle, \quad (22)$$

which has the form of an entangled state because different values of the electronic kinetic momentum lead to different effects on the field modes. Let us restrict now, for the sake of simplicity, to a 1D scenario, and to the case where only electrons of a well-defined energy are emitted. Then, the previous state could be written as $|\psi(t)\rangle = |\mathbf{v}\rangle |\Phi(\mathbf{v},t)\rangle + |-\mathbf{v}\rangle |\Phi(-\mathbf{v},t)\rangle$, and the amount of

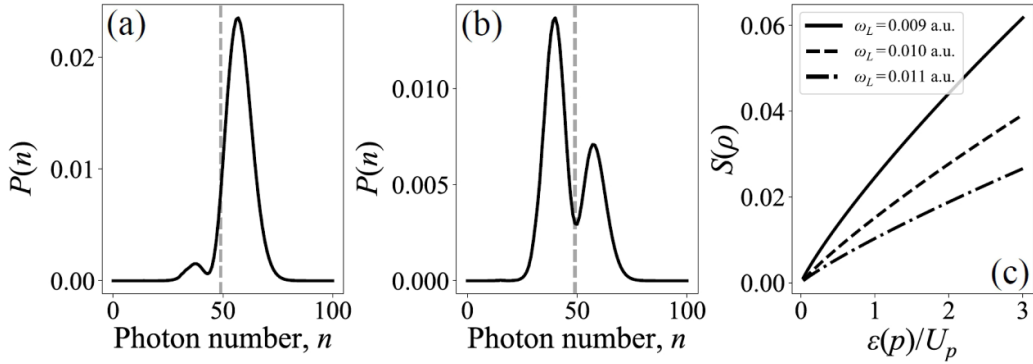


Figure 13. In (a) and (b), we show the photon number probability for two values of momentum, (a) $p = 0.32\sqrt{U_p}$ and (b) $p = -0.32\sqrt{U_p}$, where $p = mv - eA(t)/c$ is the canonical momentum. For representation purposes, the initial coherent state of the system has been set to $|\alpha_L| = 7$. In (c), we show the entropy of entanglement $S(\rho)$ as a function of the photoelectron energy $\mathcal{E}(\rho)/U_p$ for three different frequencies, $\omega_L = 0.009$ a.u. (solid curve), $\omega_L = 0.010$ a.u. (dashed curve) and $\omega_L = 0.011$ a.u. (dash-dotted curve). ((a) and (b)) Reproduced from [98]. CC BY 4.0. (c) Reprinted (figure) with permission from [105], Copyright (2022) by the American Physical Society.

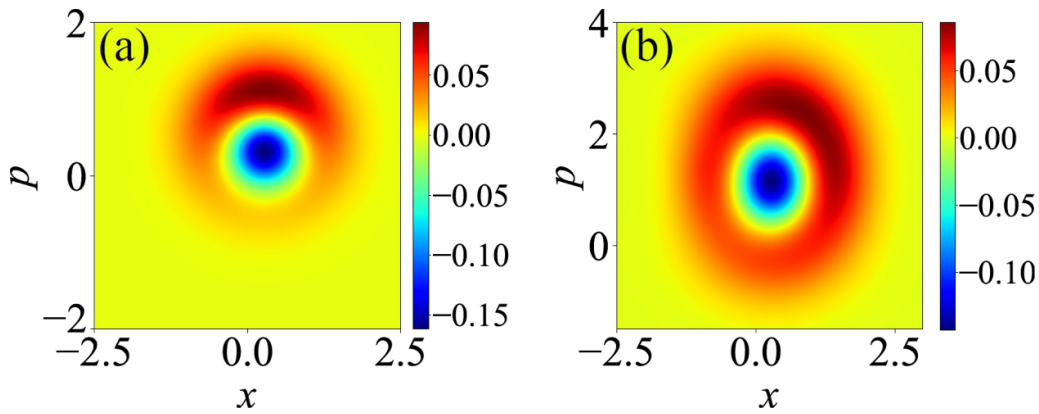


Figure 14. Calculated Wigner functions $W(x,p)$ of the fundamental driving mode when conditioned on ATI processes. (a) Conditioned on all electron momenta (equation (23)). (b) Conditioned on specific electron momentum (equation (20)). Reprinted (figure) with permission from [53], Copyright (2022) by the American Physical Society.

entanglement in it can be quantified in terms of the entropy of entanglement $S(\rho) = -\text{tr}(\rho \log_2 \rho)$ [190–192], with ρ the reduced state of the system with respect to one of the parties. In figure 13(c), $S(\rho)$ is shown as a function of the photoelectron's energy $\mathcal{E}(\rho)$ for an SAE, and for three different frequencies that belong to the MIR regime, when using a field with five optical cycles. Within this range, the values of $|\delta_1(v, t', t)|$ become big enough when considering currently available field intensities for the corresponding frequency regime [105]. As observed, the amount of entanglement increases the bigger the value of the photoelectron's energy is, and gets enhanced the more time the electron spends oscillating in the field, i.e. the lower the frequency for fields with the same number of cycles. An important feature, required to obtain these entangled states, is that the process of emitting an electron with positive and negative momentum has to be equally probable. In other words, the photoelectron spectrum needs to be symmetric. Otherwise, one of the components will dominate over the other, which makes the final state of the system to be separable. This sort of symmetricity can be found when driving the system with multicycle laser pulses, that is, when the CEP effects become negligible, while in the case of laser pulses

with few optical cycles this is not the case anymore [69, 193] (see figure 8(b)). Finally, note that when the final state of the electron cannot be discerned, the quantum optical state is left in a mixed state of the form,

$$\rho(t) = \int d\mathbf{v} |\Phi(\mathbf{v}, t)\rangle \langle \Phi(\mathbf{v}, t)|. \quad (23)$$

Figure 14, shows representative examples of the Wigner functions of the state of the fundamental driving mode in case of conditioning on all (figure 14(a)) and specific electron momenta (figure 14(b)), respectively. In the case of conditioning on all specific electron momenta, the shape of $W(x,p)$ in figure 14(a) is very similar to an optical ‘cat’ state generated when the IR field state is conditioned on HHG. This is valid under the following approximations: (i) during the ATI process the harmonic coherent-state amplitudes stay very close to the vacuum, and (ii) that the generated coherent shifts are identical and time-independent. However, the situation changes drastically in case of conditioning on specific electron momentum. In this case the $W(x,p)$ significantly deviates from the Wigner function of an optical ‘cat’ state generated by conditioning on

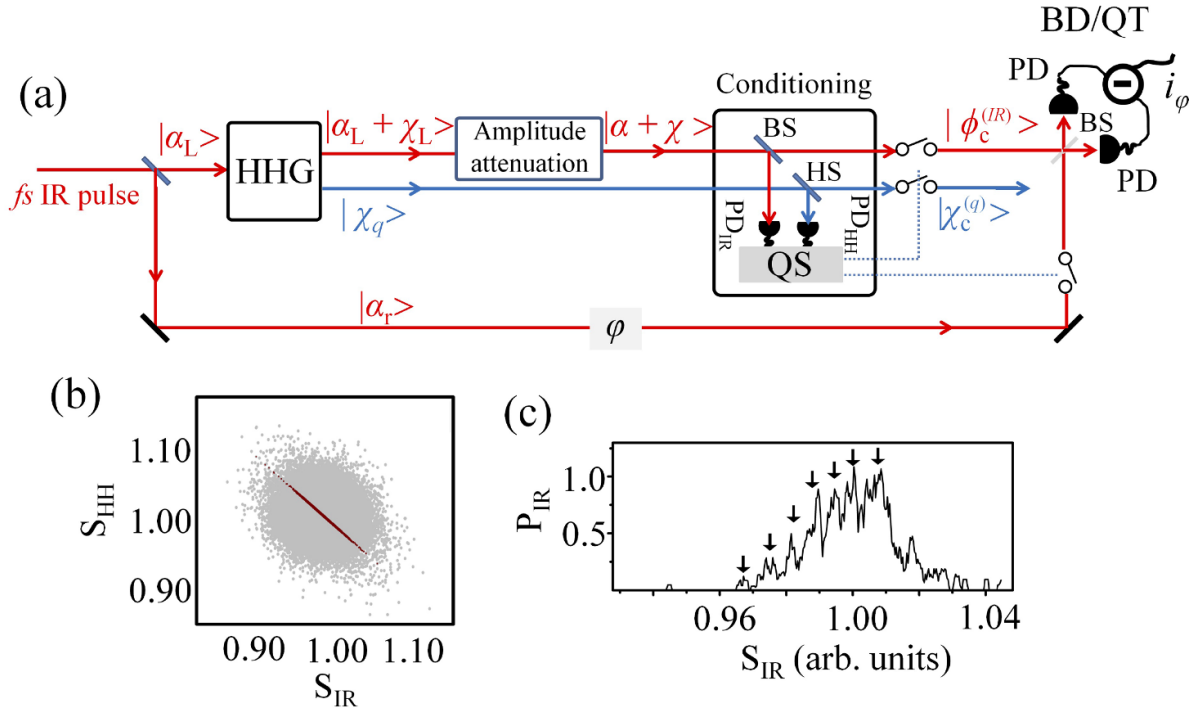


Figure 15. A schematic which shows the operation principle of the experimental approach. $|\alpha_L\rangle$ is the initial coherent state of the driving field. $|\alpha_L + \chi_L\rangle$, $|\alpha + \chi\rangle$ are the states of the IR field after the interaction and attenuation, respectively. $|\chi_q\rangle$ are the coherent states of the harmonic (q is the harmonic order). $|\phi_c^{(IR)}\rangle$ and $|\chi_c^{(q)}\rangle$ are the field states conditioned on HHG, which correspond to a coherent state superposition. BD/QT is a balanced detector (BD) of the homodyne detection system used for the characterization of the state $|\phi_c\rangle$ via quantum tomography (QT). i_φ is the φ dependent output photocurrent difference used for the measurement of the electric field operator and the light state characterization via the reconstruction of the Wigner function. $|\alpha_r\rangle$ is the state of the local oscillator reference field, with a controllable phase shift φ . PD are identical IR PDs and PD_{HH} is an HH photodetector. BS is a beam splitter. S_{IR} and S_{HH} are the signals of the PD and PD_{HH} , used for the conditioning on HHG. HS is a plane mirror, named harmonic separator. HS, in combination with spectral filtering optical elements, can be used to reflect either all or part of the high harmonics towards PD_{HH} . Quantum spectrometer (QS) is the approach used to condition the field states on the HHG process. (b) (S_{HH} , S_{IR}) photon number distribution (gray points). The mean values of (S_{HH} and S_{IR}) are normalized to 1. The red points show the selected points along the anticorrelation diagonal. (c) Probability of absorbing IR photons (P_{IR}) towards HHG. The arrows depict the positions of the peaks in the multi-peak structure of P_{IR} . Reproduced from [98]. CC BY 4.0.

HHG. This is because the final state is given as a superposition of different coherent states (which, in principle, is larger than two), where each of them is affected by the instantaneous value of the electric field operator evaluated at time t' . The shape of $W(x, p)$ in figure 14(b) is related to a change in the phase of the coherent states appearing in the superposition. However, it may also be associated with small rotations relevant to a change in the phase of the respective amplitudes in the state superposition, which at the end is related on how we are implementing the conditioning operations. Details on this matter can be found in [53].

4.2. Experimental approach: Generation of optical ‘cat’ states

In this subsection we will discuss the operation principle of an experimental approach that can be used for the implementation of the aforementioned theoretical findings. The scheme, shown in figure 15(a), allows for: (a) the generation of the non-classical light states by implementing conditioning approaches on the field modes after the interaction, (b) the control of the quantum features of the generated non-classical light states, and (c) the characterization of the quantum states of light. The

approach has been successfully used for the generation and the characterization of high photon number controllable optical ‘cat’ states using strongly laser driven atoms and conditioning on HHG [52, 53, 98].

Briefly, a linearly polarized IR fs laser pulse is focused with an intensity $I_{IR} \sim 10^{14} \text{ W cm}^{-2}$ into an atomic gas leading to the generation of high harmonic photons, ions and photoelectrons (not shown in the figure 15(a)). The coherent state of the driving laser field before the interaction is $|\alpha_L\rangle$. The state of the field during the interaction with uncorrelated atoms (as are the atoms in a room temperature gas medium) remains coherent, but is modified with an amplitude shift to lower values. Therefore, the state of driving field after the interaction is an amplitude-shifted state $|\alpha_L + \chi_L\rangle$ and the generated harmonics are in coherent state $|\chi_q\rangle$. Then, the mode of the driving field is attenuated (resulting to $|\alpha + \chi\rangle$) in the range of few-photon and conditioned to HHG by means of QS method [52, 53, 98–101]. The QS is a shot-to-shot IR vs HH photon correlation-based method, which selects only the IR shots that are relevant to the harmonic emission (figure 15(b)). It relies on photon statistics measurements and energy conservation, i.e. q IR photons need to be absorbed from the IR field for the generation of a photon of the q th harmonic. The output of

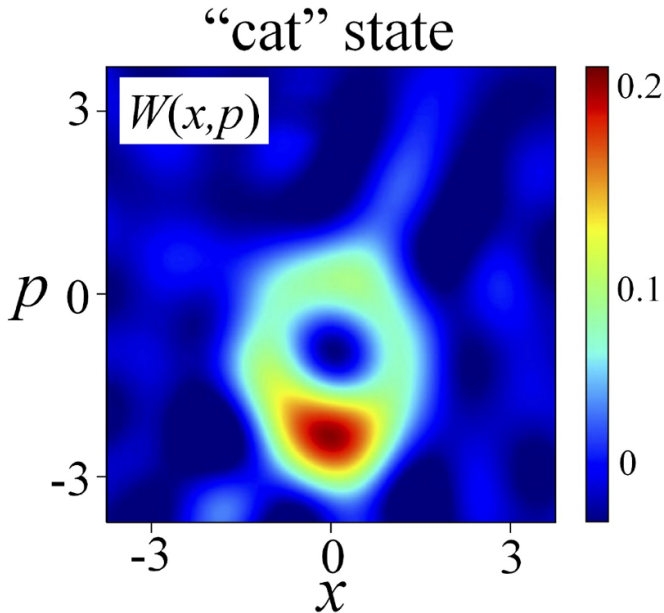


Figure 16. Measured Wigner function $W(x,p)$ of an IR optical ‘cat’ state generated by conditioning on the HHG process. The measurement is in agreement with the Wigner functions obtained by theoretical calculations of a ‘cat’ state with $|\alpha| = 2$ and $|\chi| = 1.5$ where $\xi \approx 0.32$. Reproduced from [52], with permission from Springer Nature.

the QS contains only the IR shots along the anti-correlation diagonal (figure 15(c)). By selecting these points, we condition the IR field state exiting the medium on the HHG process. This is because we select only those shots that are relevant to the harmonic emission, and we remove the unwanted background associated with all residual processes, e.g. electronic excitation or ionization. This action corresponds to the application of the $\Pi_{\tilde{n} \neq 0} = \mathbb{1} - \Pi_0$ operator onto the field state given by equation (14), and its projection onto the harmonic field modes equation (15) [102, 103]. This results in the creation of an IR field coherent state superposition (equation (15)) i.e. an optical Schrödinger ‘cat’ state of the form,

$$|\phi_c^{(\text{IR})}\rangle = |\alpha + \chi\rangle - \xi |\alpha\rangle. \quad (24)$$

The quantum character of this state can be obtained by the measurement of its Wigner function. Figure 16 shows the measured Wigner function of an IR optical ‘cat’ state that has been generated by conditioning on the HHG. In this experiment, the high harmonics have been generated by the interaction of Xenon atoms with an ≈ 30 fs IR pulse of intensity $I_L \approx 8 \times 10^{13} \text{ W cm}^{-2}$. For the conditioning, the harmonics with $q > 11$ (i.e. mainly the plateau harmonics) have been used.

4.2.1. Controlling the quantum features of the optical ‘cat’ states. The experimental approach discussed in section 4.2, has been used for the generation of high-photon number shifted optical ‘cat’ states and coherent state superposition with controllable quantum features using intense laser–atom

interactions [52, 53, 98]. The control of the quantum features is shown in figure 17, where an optical ‘cat’ state switches to a ‘kitten’ for lower values of χ . The value of χ can be controlled by changing the gas pressure in the interaction area (equation (13)). As is shown in section 4.1.3 the same approach can be used for conditioning on ATI [53, 98], and, in principle, can be extended to two-electron ionization processes, etc. This, besides its fundamental interest associated with electron-photon correlation during the ATI/HHG process, provides an additional ‘knob’ of controlling the quantum character of the optical ‘cat’ states, a feature extremely valuable for applications in quantum technology. Also, as it was discussed in section 4.1.2, single and two-color driven laser–atom interactions can result in the generation of ‘massively’ entangled optical coherent states in the spectral range from XUV to the far–IR. Such states in combination with passive linear optical elements (such as phase shifters, BSs, and optical fibers) [98] can be considered as unique resources for novel applications in quantum technology.

4.3. Extension to interactions with complex materials and generation of massively entangled states

The process of HHG has been observed when a strong laser field drives all states of matter. It has been observed in strongly laser driven molecules, clusters, liquids, semiconductor materials, nanostructures, 2D materials, solid-surfaces via laser-plasma interactions [81, 83, 194, 195], and very recently in quantum correlated materials such as high temperature superconductors [196]. The arrangement used for investigating these interactions is based on the schematic shown in figure 6. It is noted that in case of interactions with solid surfaces [81, 195], the driving laser field and the high harmonics are reflected from the target area (not shown in figure 6). The intensity of the laser pulse in the interaction region depends on the properties of the target. Typically is $I_L > 10^{11} \text{ W cm}^{-2}$ for solid state and 2D materials, $I_L > 10^{14} \text{ W cm}^{-2}$ for atoms (such as Noble gases) and molecules (mostly diatomic), and $I_L > 10^{18} \text{ W cm}^{-2}$ for laser–plasma interactions on solid surfaces.

In the majority of the aforementioned interactions, the HHG process has been described by semi-classical methods, which in many cases rely on the extension/modification of the methods developed for the description of intense laser–atom interaction (see section 3). Although the fully quantized description of these interactions requires a detailed study (for example in atomic and molecular targets one can use TDSE or SFA [83], for solids sometimes semiconductor Bloch equations, and for strongly correlated systems more sophisticated methods), it can be considered that, in principle, they have the potential to serve as additional resources for engineering non-classical and entangled states using the approach described in section 4.2. This is because in all these interactions:

- The driving field before the interaction is in a coherent state $|\alpha_L\rangle$.

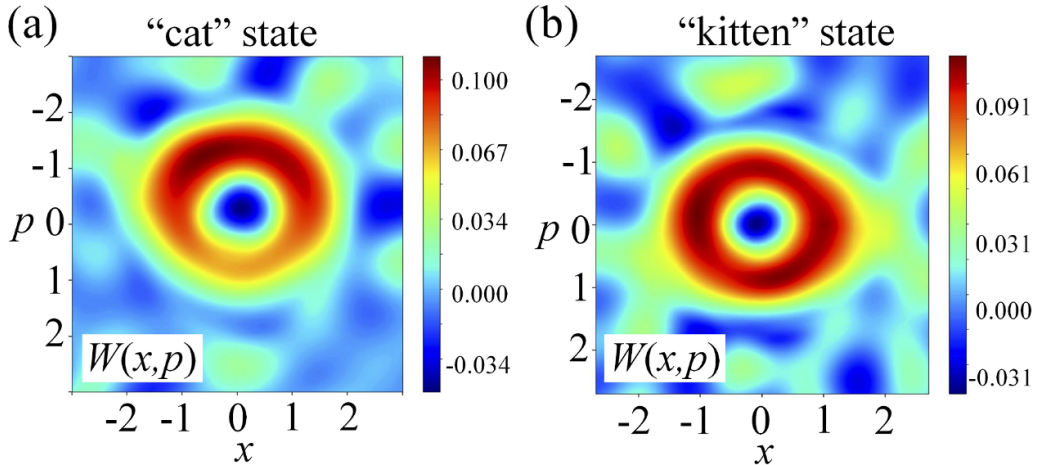


Figure 17. Measured Wigner functions $W(x,p)$ of an IR optical ‘cat’ (a) and ‘kitten’ (b) state, respectively. Optical ‘cat’ and ‘kitten’ states are created by conditioning on HHG for different values of $|\chi|$. The measurement is in agreement with the Wigner functions obtained by theoretical calculations of a ‘cat’ state with $|\alpha| = 1.4$ and $|\chi| = 0.5$ where $\xi \approx 0.88$ and a ‘kitten’ state with $|\alpha| = 1.3$ and $|\chi| = 0.1$ where $\xi \approx 0.99$. Reprinted (figure) with permission from [53], Copyright (2022) by the American Physical Society.

- After the interaction, the energy conservation suggests that the state of the driving field mode is an amplitude-shifted coherent state $|\alpha_L + \chi_L\rangle$, and the emitted high harmonics are in a coherent state $|\chi_q\rangle$. We note that in the case of interactions with quantum correlated materials the outgoing for interaction field modes (fundamental and harmonic) could be in non-classical states [197].
- After the interaction, the fundamental laser field can be attenuated in a coherent manner in the range of few–photons and conditioned to HHG by means of QS. This will result in the creation of non-classical light states.

Such investigations have been already started in strongly laser driven semiconductors [198, 199]. In this case, an electron may tunnel out from a parent atom (a parent site in the lattice) and recombines on another atom (another site). If the dynamics on the valence band is slow, this situation rarely happens and the physics is very similar to that of atoms. *Quantumness* can be generated using conditioning. If the valence intraband dynamics is faster, it may lead to noticeable entanglement between electron final position and light and non-classical states of light without the need for conditioning, which, however may augment the quantum effects. If the valence intraband dynamics is too fast, electron may recombine anywhere with random phase, which leads to strong decoherence and the impossibility of efficient phase matching of harmonics [200].

Also theoretical investigations in strongly laser driven quantum correlated materials [197, 201], and proposals towards the implementation of the approach in relativistic laser plasma interactions [202] have been reported. Furthermore, recent developments on the generation of high intensity squeezed light sources [203–206] have initiated experimental and theoretical investigations on the influence of the quantum features of these light states on the multi-photon processes [204, 205], as well as, theoretical studies on the influence of the quantum noise of a squeezed light field on the HHG process [207, 208].

Taking into account the high photon number of the driving field and the large number non-classical field–modes (fundamental and harmonics) generated using the aforementioned methods, it can be considered that the strongly laser-driven materials is an ideal resource for engineering massively quantum correlated states which is of fundamental importance for QI science and quantum technologies.

5. Applications in QI science

Contemporary quantum technologies face major difficulties in fault tolerant quantum computing with error correction, and focus instead on various shades of quantum simulation (Noisy Intermediate Scale Quantum, NISQ) devices [209], analog and digital quantum simulators [210] (for a recent report on progress including quantum computing and quantum simulation, see [211]), and quantum annealers [212]. There is a clear need and quest for systems that, without necessarily simulating quantum dynamics of some physical systems, can generate massive, controllable, robust entangled and superposition states. This will, in particular, allow for the use of decoherence in a controlled manner, enabling the use of these states for quantum communications [213] (e.g. to achieve efficient transfer of information in a safer and quicker way), quantum metrology [56], sensing and diagnostics [214] (e.g. to precisely measure phase shifts of light fields, or to diagnose quantum materials).

As we discuss in this report, QED of SLP, combined with QO, leads to non-trivial applications in QI science. Indeed, it offers a set of stable and reproducible methods to generate massively entangled states and massive quantum superpositions [52, 53, 98, 103]. In this section we discuss that in fact there are more new paths for QI science via the symbiosis with AP and QO. These studies concern, in the first place, the fundamental QI science, but aim at quantum technologies. They deal in particular with: (i) Detection of topology, strongly correlated systems, chirality, etc (see [196, 215]); (ii)

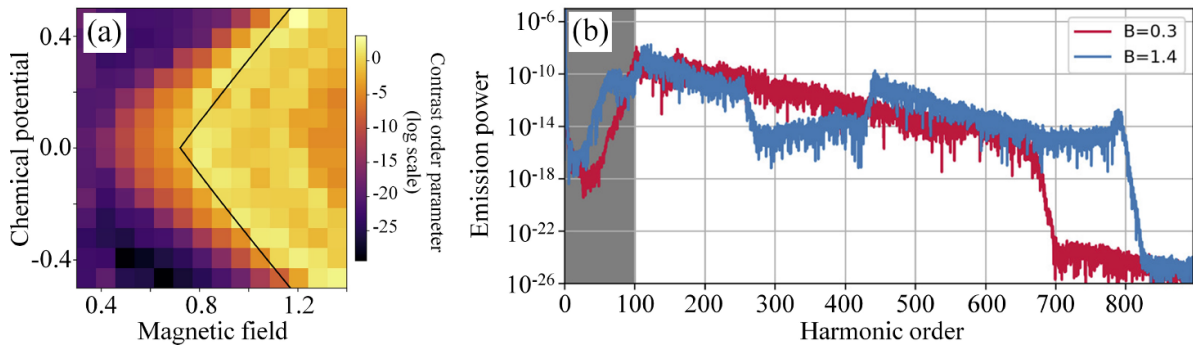


Figure 18. (a) The phase diagram of the proximity-induced p-wave superconductor is obtained from an order parameter based on the harmonic emission spectrum, shown in (b) for two parameter choices, in the topological and in the trivial phase. At frequencies below the band gap, emission is suppressed in the trivial phase (red), whereas in the topological phase emission is possible already at frequencies above half the band gap due to the edge state in the middle of the band gap. Reproduced with permission from [215]. Copyright © 2022 The Authors. Published by American Chemical Society. CC BY-NC-ND 4.0.

Generation of topology, strongly correlated systems, chirality, etc (see [216]); (iii) Generation of entangled/quantum correlated states using conditioning methods (see [52, 53, 98, 199]); (iv) SLP and AP driven by non-classical light; (v) Studies of quantum correlated states/decoherence in *Zerfall* processes (see [182]).

5.1. Detection of topology, strongly correlated systems, chirality, etc

Recently, there is an explosion of interest in applying AP methods to diagnose and detect topological order, strongly correlated systems, and chirality. The primary role is played here by the process of HHG. This is important for QI science at least for two reasons: i) combined with conditioning methods, this will definitely lead to novel ways of generating massive entanglement and massive quantum superpositions; ii) strongly correlated material exhibit themselves many-body entanglement; strongly correlated topological or chiral materials typically long range entanglement [217]—HHG will possibly allow to detect and characterize it.

5.1.1. Detection of topological order with HHG. The pioneering work of Huber *et consortes* [218] studied lightwave-driven Dirac currents in a topological surface band. ‘Harnessing the carrier wave of light as an alternating-current bias may enable electronics at optical clock rates’ [218–221]. In these papers the authors observe directly how the carrier wave of THz light pulse accelerates Dirac fermions in the topological state of Bi_2Te_3 .

The first papers, where HHG was used for the detection of topology, were the series of papers by D. Bauer with his collaborators on the detection of topological edge states in dimerized chains [222, 223], first using a self-consistent time-dependent density functional theory approach. For harmonic photon energies smaller than the band gap, the harmonic yield was found to differ by 14 orders of magnitude for the two topological phases. Similar conclusions were obtained for Su-Schrieffer-Heeger chains that display topological edge states. Recently, this method has been extended to the detection of

Majorana fermions in the Kitaev chain [224] and in quantum wires with proximity-induced p-wave superconductivity [215] (see figure 18). Specifically, the harmonic emission spectrum in strong fields was shown to exhibit spectral features due to radiating edge modes, present in the topological phase, and absent in the trivial phase. The results suggest HHG spectroscopy as a novel all-optical tool for the detection of, still controversial, Majorana zero modes.

In the seminal *Nature Photon.* paper, Ivanov *et consortes* discussed topological strong-field physics on sub-laser-cycle timescale [225]. These authors studied the response of the Haldane model [226] to ultrashort, ultrastrong laser pulses. They demonstrated that electrons tunnel differently in trivial and topological insulators due to the key role of the Berry curvature. Attosecond delays and helicities of harmonics serve then to the phase diagram of the system. Strong fields can also be used for manipulations of topological properties of 2D materials, relevant for valleytronic devices [227]. Chacón *et al* [228] obtained complementary results studying circular dichroism, which clearly heralded topological phases and transitions in the Haldane model and other Chern insulators.

5.1.2. Detection of strongly correlated systems with HHG. This is another rapidly developing area. As pointed out in the recent review [229]: ‘A hallmark effect of extreme nonlinear optics is the emission of high-order harmonics of the laser from the bulk of materials. The discovery and detailed study of this phenomenon over the course of the past decade has offered a broad range of possibilities and seen the dawn of a new field of extreme solid-state photonics. In particular, it opens the way to previously inaccessible spectral ranges, as well as the development of novel solid-state spectroscopy and microscopy techniques that enable detailed probing of the electronic structure of solids.’

Pioneering studies of HHG in strongly correlated materials are described in the paper by Silva *et al* [201], where the HHG is used to time-resolved ultrafast many-body dynamics of an optically driven phase transition to Mott insulator. Further studies on two-dimensional Mott insulators were carried out by Orthodoxou *et al* using quantum Monte Carlo,

exact diagonalization, and a simplified dynamical mean-field model [230]. The theory on HHG from Mott insulators was also reported recently by the Tokyo group, who used infinite time-evolving block decimation method and exact diagonalization [231, 232], and more recently, together with Werner demonstrated anomalous temperature dependence of HHG in Mott insulators. This reveals the crucial effect of strong spin-charge coupling on HHG in Mott insulators. In a system with antiferromagnetic correlations, ‘the HHG signal is drastically enhanced with decreasing temperature, even though the gap increases and the production of charge carriers is suppressed. This anomalous behavior, which has also been observed in recent HHG experiments on Ca_2RuO_4 [233], originates from a cooperative effect between the spin-charge coupling and the thermal ensemble, as well as the strongly temperature-dependent coherence between charge carriers’ A bosonic analog of fermionic HHG in a strong time-dependent synthetic vector potential has also been theoretically investigated by Roy *et al* [234] as a phase distinction measure to distinguish between the Mott and the superfluid phase. HHG has even been proposed to be used as a probe to identify dynamic features of hard to measure quantum spin liquids, as the magnetic-field dependence of the HHG spectra can drastically differ from those of usual ordered magnets [235].

Ultrafast laser and HHG based solid state spectroscopic techniques have increasingly become popular. Polarization-state-resolved high-harmonic spectroscopy of solids was reported in [236]. Ultrafast pump-probe spectroscopy has been used to detect the presence of Hubbard excitons in certain Mott insulators [237]. Femtosecond optical pulses have also been used to stabilize non-thermal transient phases lasting few picoseconds in the Mott-Hubbard insulator di-Vanadium trioxide [238]. In [239], the authors establish time-resolved HHG for tracking photo-induced dynamics of the insulator-to-metal phase transitions in vanadium dioxide. Closely, related to this is the study by Johnson *et al* where they use time and spectrally resolved coherent x-ray imaging to track the light-induced insulator-to-metal phase transition in vanadium dioxide on the nanoscale with femtosecond time resolution [240] and also observed the ultrafast loss of lattice coherence in the light induced structural phase transition of di-Vanadium trioxide [241].

Studies of the detection of Majorana fermions [215, 224] should also be mentioned in this context. MBI groups of Ivanov and Smirnova studied the strong laser field response of the two-band Hubbard model, using advanced techniques of dynamical mean field theory ([242], see also M. Ivanov’s contribution to [243]). In this work, the authors introduced a new type of non-linear approach that allows unraveling the sub-cycle dynamics of strongly correlated systems interacting with few-cycle IR pulses. Their approach can resolve pathways of charge and energy flow between localized and delocalized many-body states in the 2D Hubbard model; it allows also to describe the creation of highly correlated states that survive after the end of the laser pulse.

Other applications of HHG to strongly correlated materials and condensed matter systems include: (i) extraction of higher-order nonlinear electronic response in solids [244];

(ii) HHG enhancement in solid state nano-structures, such as graphene heterostructures [245]; (iii) characterization of quantum criticality in strongly correlated systems [246]: In the latter work exact diagonalization method was applied for the extended Hubbard model on a periodic chain. It was shown that HHG close to the quantum critical point, is more efficient than in the gapped charge-density-wave and spin-density wave phases; (iv) Ohio group led by Landsmann [247] studied ultra-fast laser-driven dynamics in metal–insulator interface using HHG, and showed the field induced dielectric break-down at the Mott-insulator/metal interface. They demonstrated that the intensity of high harmonic emission correlates closely with double production and the corresponding loss of short-range anti-ferromagnetic order.

HHG has also studied in cuprates (YBCO) in a broad temperature range from 80 K to 300 K, probing different phases of the high- T_c material [196]. Amazingly, HHG differs in various strongly correlated phases: The superconducting phase is marked by a strong increase of emission at all odd harmonic frequencies (3rd, 5th, and 7th), whereas the transition from the pseudogap phase to the strange metallic phase is reflected by an intensity drop only in the highest harmonics (7th). The experimental results were reproduced by simulating a two-band model in the d-wave paring mean-field regime, including phenomenological scattering terms. In another study [248], using terahertz (THz) two-pulse coherent spectroscopy, coherent oscillation of the complex amplitude mode or Higgs mode has been observed in an iron-based superconductor, thus paving the way for light-based control of the Higgs mode, an illusive mode which is notoriously difficult to detect due to its non-linearly coupling with the electromagnetic field.

Clearly, it is already possible to image and manipulate strongly correlated materials with HHG at optical rates for ultrashort laser pulses, far beyond Floquet engineering of quantum systems. For future QI applications, it is important to remember that in all these processes it is natural to expect the generation of massively entangled states of matter, light, and light-matter. Indeed, recently Pizzi *et al* [197] proposed a quantum-optical theory of a strongly driven many-body system, showing that the presence of correlations among the emitters creates emission of many-photon states of light which deviate from the coherent states of light. The authors considered a simplified model of matter, described by a quadratic Hamiltonian, and took as an example HHG. They demonstrated that a correlation of the emitters prior to the strong drive is converted onto features different from coherent radiation of the output light, including doubly-peaked photon statistics, ring-shaped Wigner functions, and correlations between harmonics (for a description for a general audience, see [249] and (figure 19)). However, genuine non-classicality in the properties of the emitted radiation is still not unambiguously present.

5.1.3. Detection of chirality with HHG. The detection of chirality is somewhat similar to the detection of topological order with HHG, but nowadays mostly refers to molecular targets. Chirality is generic for biological molecules; distinguishing

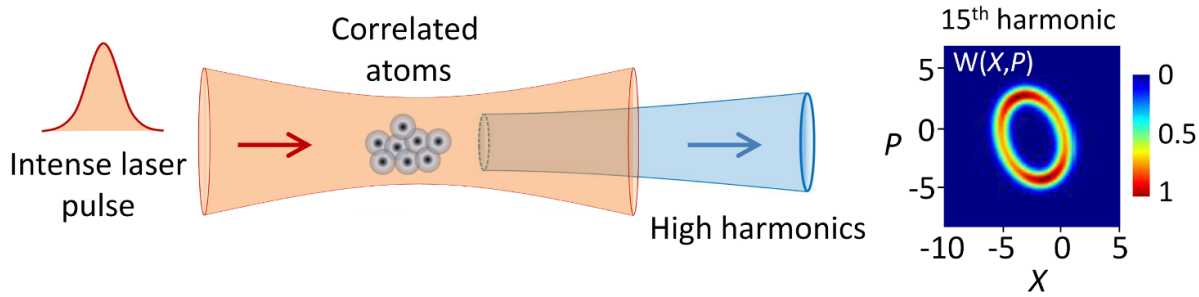


Figure 19. Strongly laser-driven quantum correlated many-body systems lead to the generation of light with exotic quantum features—the quantumness of a many-body system is imprinted on the state of the emitted light. Figure reproduced from [249] which refers to the findings of [197]. Reproduced from [249], with permission from Springer Nature.

molecules which differ only by their chirality has a gigantic technological importance which cannot be overstated. The relevance for QI science concern here additionally two aspects: (i) Molecules (chiral or not) offer novel ways of generating entangled states, similar to those discussed for solids [199], where an electron localized close to one nucleus, recombines on the other; (ii) possibility of generalizing chirality imaging to many-body chiral systems.

In recent years, O Smirnova and collaborators obtained numerous seminal results concerning ultrafast imaging of chiral molecules (see [250], see [251] for a recent review). In [252, 253] the authors introduced the concept of *locally chiral light*, i.e. light that is chiral within the electric-dipole approximation by means of its 3D chiral Lissajous figure. This type of chiral light can be synthesized and exploited to dramatically enhance the contrast between HHG spectra in molecules with opposite chiralities. In [254], they study the transverse spin of the light, which emerges whenever light is confined to a small region of space in ultra-fast chiral imaging. This results in harmonics with a polarization that depends on the molecular chirality. The effects of synthetic chiral light also extend to other attosecond-science properties, such as the use of a chirally-sensitive nonlinear Stark shift to deflect free-induction decay radiation in an enantiosensitive fashion [255].

Recently, we found [256] that chiral molecules subject to strong-field ionization with a few-cycle, IR, linearly polarized pulse emit *twisted* photoelectrons with the twist (OAM) depending on the molecular chirality. This effect, termed *photoelectron vortex dichroism*, offers novel ways of imaging chirality, and suggests intriguing perspectives regarding the role of the electron OAM in recollision-based phenomena in chiral molecules.

5.2. Generation of topology, strongly correlated systems, chirality, etc

As discussed above, AP and HHG serve as great detection tools; amazingly, ultrafast laser pulse and attophysics methods may also be used for the generation of topological order, strongly correlated states, chirality, etc. In all these cases we foresee the possibility of the generation of novel entangled states of light, matter, and light-matter, relevant for QI science.

The ideas reported here are, of course, close to the attempts to generate room temperature high T_c superconductivity [257], or Chern insulators [258], which belong more to the domain of ultrafast, but THz physics.

A good example of laser-induced phase transitions is discussed in the experimental group of S. Wall on THz field control of in-plane orbital order in $\text{La}_{0.5}\text{Sr}_{1.5}\text{MnO}_4$ [259]. We have also started to investigate possibilities of laser induced fluctuating bonds in superconductivity [260] in hole-doped cuprates. In the recent Phys. Rev. B Lett. [216], demonstrating the theoretical possibility of generation of fermionic Chern insulators from twisted light with linear polarization in graphene-like materials.

A particularly interesting line of research, connects generation of topology, strongly correlated systems, chirality etc with the use of more complex *structured laser light*, combining polarization and OAM effects. A perfect example is a superposition of left and right circular polarized two-color laser fields in a, so-called, MAZEL-TOV configuration [165, 173]. Such driving leads to the famous three-foil Lissajous patterns of the electric field, and efficient generation of circularly polarized high harmonics.

Another example is the light, which forms fractional-order knots in the dynamics of the electric field vector employing the polarization state of light and superposition of the fundamental and doubled frequency [261]. Application of strong laser pulses of this form to atomic targets leads to ‘exotic’ conservation of torus-knot angular momentum in high-order harmonic generation [169]. Combining two delayed circularly polarized pulses of frequency ω and 2ω , one can generate light with a self-torque: extreme-ultraviolet beams of HHG with time-varying OAM [177]. Combining structured laser light with conditioning opens new possibilities of generating massive entanglement and superpositions with a topological ‘touch’ – so far not yet explored areas for QI application.

As shown in [262], *locally chiral light* [252, 253], another type of structured light, can be used to efficiently (i.e. at the level of the electric-dipole approximation) imprint 3D chirality on achiral matter, such as atoms. Locally chiral light sculpts a chiral orbital out of the initially achiral ground state, exciting the electron into an orbital with a chiral shape.

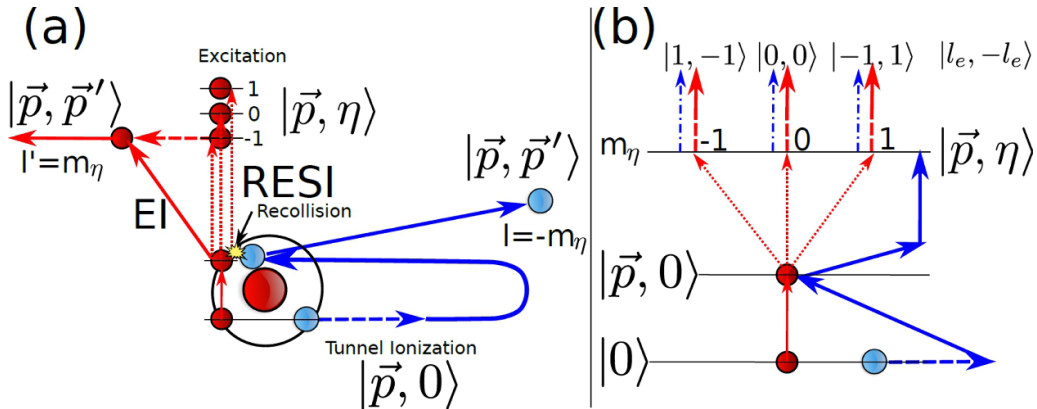


Figure 20. Non-sequential double ionization (NSDI), a ‘Zerfall’ processes, leading to entanglement between the orbital angular momentum (OAM) of the two photoelectrons. In panel (a), an electron is ionized via a strong laser field and recollides with the parent atom/molecule. This leads to either: direct ionization of a second electron in electron impact (EI) ionization, or excitation with subsequent ionization (RESI) of a second electron. Panel (b) focuses on RESI, the OAM superposition in the excited state is transferred to the final state along with anti-correlation between the electrons. The figure is reproduced from [272] reporting on result from [182], which contained a similar figure. Reproduced from [272]. CC BY 4.0.

5.3. Strong-field physics and atto-second science driven by non-classical light

All the quantum optical studies of strong field driven processes have thus far been approached by assuming a coherent state description for the driving field. The corresponding field is classical, even if Hilbert space methods are used for its description. However, in a recent work, presented at ATTO VIII by Even Tzur *et al* [263], this assumption was abandoned, and the process of HHG driven by non-classical light fields has been presented for the first time. In the recent paper [264] they show that the plateau and cutoff in HHG spectrum are sensitive to the photon statistics of the driving light. While coherent (classical) and Fock light states induce the established HHG cutoff law, thermal and squeezed states substantially surpass it. This opens the path for investigating the interplay between non-classical properties of the driving source, and quantum properties of the harmonic modes. In another paper [207] they also show, using a quantum generalization of SFA, that dynamics of matter driven by bright (intense) light significantly depend on the quantum state of the driving light, which induces an effective photon-statistics force. It is worth mentioning that these works go back to an earlier paper on ‘Compton Scattering Driven by Quantum Light’ [265], where the authors obtain analytical results for the Compton emission spectrum when driven by thermal and squeezed vacuum states, showing a noticeable broadening of the emission spectrum relative to a coherent drive, thus reaching higher emission frequencies for the same average intensity.

5.4. Generation of entanglement in Zerfall processes

Finally, AP is a perfect playground to study the generation of quantum correlations and entanglement in *Zerfall* processes, i.e. processes of decay of a ‘whole’ in products. A prime example of this is NSDI, where strong-field ionization followed by laser induced recollision leads to double ionization of the target, see figure 20(a). Strong correlation between the

ionization products, in particular the two photoelectrons, has long been known [181]. Previously, coherence and interference between the two photoelectrons has been studied in great detail [266–269]. More recently, Maxwell *et al* [182] studied generation of entanglement in NSDI, by using correlation in the OAM of the outgoing electrons, for a mini-review on OAM in strong-field ionization see [270, 271]. A key step, is to exploit the intermediate excited state, and its inherent superposition over OAM, which is present for the ‘second’ electron for the low-intensity regime¹¹. Thus, simple conservation laws dictate that the final OAM of the two electrons must be anti-correlated, which at certain final momentum leads to a maximally entangled qutrit, see figure 20(b), while remaining robust to incoherent effects, such as focal averaging or decoherence with the ion.

Continuum products in a *typical* strong-field Zerfall processes will be quantified through continuous variables, which can complicate analysis of entanglement measures. However, the use of OAM makes the task of quantifying and measuring entanglement much easier, the computations of the reduced density matrix of ionized product in the OAM space become simple, and in the case of NSDI, clearly exhibit entanglement. This also enables quantification by the, so-called, logarithmic negativity, which may be used for mixed states to model incoherent effects.

5.5. Characterizing decoherence in Zerfall processes

Finally, studies of *Zerfall* processes offer a unique opportunity to understand and characterize quantum and classical decoherence. This goes back to seminal and pioneering theoretical works by Santra *et al* [273–275], Lara-Astiaso *et al* [276], or Vacher *et al* [277]. All of these works dealt essentially with the single electron ionization process that

¹¹ This is known as the recollision with subsequent ionization (RESI) mechanism.

might lead to entanglement of the electron with the parent ion. Measuring the reduced density matrix of the electron provides thus information about decoherence and thus entanglement Vrakking *et al* has developed both theoretical and the first experimental ideas in this context [278, 279] (see also Vrakking's contribution to [243]). One of the main problems in this line of research is to make sure that the source of decoherence is truly quantum. Indeed, by analyzing with great care various classical and quantum models of decoherence in the process of single electron ionization, Bourasson-Bouchet *et al* demonstrated dominantly classical sources of decoherence.

In contrast, in the recent work [280], L'Huillier *et al* investigated decoherence due to entanglement of the radial and angular degrees of freedom of the photoelectron. They study two-photon ionization via the $2s2p$ autoionizing state in He using high spectral resolution photoelectron interferometry. Combining experiment and theory, we show that the strong dipole coupling of the $2s2p$ and $2p^2$ states results in the entanglement of the angular and radial degrees of freedom. This translates, in angle-integrated measurements, into a dynamic loss of coherence during autoionization.

6. Conclusions

We report on the recent progress on the fully quantized description of intense laser–matter interactions and the development of approaches that have been used for the generation of controllable entangled and non-classical light states. This has led to the connection of strong laser field physics with QO and QI science. Specifically, after an introduction to the fundamentals of QO, non-classical light engineering and intense laser–matter interactions, we discuss the fully quantized description of intense laser–matter interaction emphasizing on QED of strongly laser–driven atoms, HHG and above threshold ionization processes. Then, we discuss the quantum operations (conditioning) used to engineer optical ‘cat’ and entangled states from the XUV to the far–IR, as well as the procedures that can be followed to control their quantum features. Additionally, we provide the perspectives towards the extension to interactions with complex materials as well as interactions with intense quantum light, that can serve as additional resources for engineering novel non-classical and entangled states. Finally, we discuss a number of applications stemming from the symbiosis of strong laser-field physics and ultrafast science with QO and QI science.

Data availability statement

No new data were created or analysed in this study.

Acknowledgments

P Tzallas group at FORTH acknowledges support from: LASERLABEUROPE V (H2020-EU.1.4.1.2 Grant No.871124), FORTH Synergy Grant AgiIDA (Grant No. 00133), the H2020 framework program for research and innovation under the NEP-Europe-Pilot Project (No.

101007417), the Hellenic Foundation for Research and Innovation (HFRI) and the General Secretariat for Research and Technology (GSRT) under Grant NEA-APS HFRI-FM17-3173, the H2020 Project IMPULSE (GA 871161) and ELI-ALPS. ELI-ALPS is supported by the European Union and co-financed by the European Regional Development Fund (GINOP Grant No. 2.3.6-15-2015-00001).

M Lewenstein group at ICFO acknowledges support from: ERC AdG NOQIA; Ministerio de Ciencia y Innovation Agencia Estatal de Investigaciones (PGC2018-097027-B-I00/10.13039/501100011033, CEX2019-000910-S/10.13039/501100011033, Plan National FIDEUA PID2019-106901GB-I00, FPI, QUANTERA MAQS PCI2019-111828-2, QUANTERA DYNAMITE PCI2022-132919, Proyectos de I+D+I ‘Retos Colaboración’ QUSPIN RTC2019-007196-7); MICIIN with funding from European Union NextGenerationEU(PRTR-C17.II) and by Generalitat de Catalunya; Fundació Cellex; Fundació Mir-Puig; Generalitat de Catalunya (European Social Fund FEDER and CERCA program, AGAUR Grant No. 2021 SGR 01452, QuantumCAT U16-011424, co-funded by ERDF Operational Program of Catalonia 2014–2020); Barcelona Supercomputing Center MareNostrum (FI-2022-1-0042); EU Horizon 2020 FET-OPEN OPTOlogic (Grant No. 899794); EU Horizon Europe Program (Grant Agreement 101080086 - NeQST), National Science Centre, Poland (Symfonia Grant No. 2016/20/W/ST4/00314); ICFO Internal ‘QuantumGaudi’ project; European Union’s Horizon 2020 research and innovation program under the Marie-Skłodowska-Curie Grant Agreement Nos. 101029393 (STREDCH) and 847648 (‘La Caixa’ Junior Leaders fellowships ID100010434: LCF/BQ/PI19/11690013, LCF/BQ/PI20/11760031, LCF/BQ/PR20/11770012, LCF/BQ/PR21/11840013). Views and opinions expressed in this work are, however, those of the author(s) only and do not necessarily reflect those of the European Union, European Climate, Infrastructure and Environment Executive Agency (CINEA), nor any other granting authority. Neither the European Union nor any granting authority can be held responsible for them.

M F Ciappina acknowledges financial support from the Guangdong Province Science and Technology Major Project (Future functional materials under extreme conditions - 2021B0301030005) and the Guangdong Natural Science Foundation (General Program Project No. 2023A1515010871).

P Stammer acknowledges funding from: The European Union’s Horizon 2020 research and innovation programme under the Marie Skłodowska-Curie Grant Agreement No. 847517.

J Rivera-Dean acknowledges support from: The Secretaria d’Universitats i Recerca del Departament d’Empresa i Coneixement de la Generalitat de Catalunya, as well as the European Social Fund (L’FSE inverteix en el teu futur)–FEDER.

A S Maxwell acknowledges funding support from: The European Union’s Horizon 2020 research and innovation programme under the Marie Skłodowska-Curie Grant Agreement, SSFI No. 887153.

E Pisanty acknowledges Royal Society University Research Fellowship funding under Grant URF/R1/211390.

Authors contributions

U B, Th L, A M, A O, E P, J R-D, P S: equally contributing authors placed in the author list in alphabetical order. M F C, M L and P T: supervised the work.

ORCID iDs

A S Maxwell  <https://orcid.org/0000-0002-6503-4661>
 A Ordóñez  <https://orcid.org/0000-0001-5274-4413>
 E Pisanty  <https://orcid.org/0000-0003-0598-8524>
 J Rivera-Dean  <https://orcid.org/0000-0003-3031-0029>
 P Stammer  <https://orcid.org/0000-0001-7137-2053>
 M F Ciappina  <https://orcid.org/0000-0002-1123-6460>
 M Lewenstein  <https://orcid.org/0000-0002-0210-7800>
 P Tzallas  <https://orcid.org/0000-0002-8063-5596>

References

- [1] Hanbury-Brown R and Twiss R Q 1956 Correlation between photons in two coherent beams of light *Nature* **177** 27
- [2] Siegman A 1986 *Lasers* (University Science Books)
- [3] Glauber R J 1963 Coherent and incoherent states of the radiation field *Phys. Rev.* **131** 2766
- [4] Glauber R J 1963 The quantum theory of optical coherence *Phys. Rev.* **130** 2529
- [5] Sudarshan E 1963 Equivalence of semiclassical and quantum mechanical descriptions of statistical light beams *Phys. Rev. Lett.* **10** 277
- [6] Chu S 1998 Nobel lecture: the manipulation of neutral particles *Rev. Mod. Phys.* **70** 685
- [7] Cohen-Tannoudji C N 1998 Nobel lecture: Manipulating atoms with photons *Rev. Mod. Phys.* **70** 707
- [8] Phillips W D 1998 Nobel lecture: laser cooling and trapping of neutral atoms *Rev. Mod. Phys.* **70** 721
- [9] Cornell E A and Wieman C E 2002 Nobel lecture: Bose-Einstein condensation in a dilute gas, the first 70 years and some recent experiments *Rev. Mod. Phys.* **74** 875
- [10] Ketterle W 2002 Nobel lecture: When atoms behave as waves: Bose-Einstein condensation and the atom laser *Rev. Mod. Phys.* **74** 1131
- [11] Glauber R J 2006 Nobel lecture: one hundred years of light quanta *Rev. Mod. Phys.* **78** 1267
- [12] Hall J L 2006 Nobel lecture: defining and measuring optical frequencies *Rev. Mod. Phys.* **78** 1279
- [13] Hänsch T W 2006 Nobel lecture: passion for precision *Rev. Mod. Phys.* **78** 1297
- [14] Haroche S 2013 Nobel lecture: controlling photons in a box and exploring the quantum to classical boundary *Rev. Mod. Phys.* **85** 1083
- [15] Wineland D J 2013 Nobel lecture: superposition, entanglement and raising Schrödinger's cat *Rev. Mod. Phys.* **85** 1103
- [16] Ashkin A 2018 Nobel lecture: optical tweezers and their application to biological systems (NobelPrize.org., Stockholm, Sweden) (available at: www.nobelprize.org/prizes/physics/2018/ashkin/lecture/) (Accessed 8 December 2018)
- [17] Mourou G 2019 Nobel lecture: extreme light physics and application *Rev. Mod. Phys.* **91** 030501
- [18] Strickland D 2019 Nobel lecture: generating high-intensity ultrashort optical pulses *Rev. Mod. Phys.* **91** 030502
- [19] Aspect A 2022 Nobel lecture: from Einstein's doubts to quantum technologies: non-locality a fruitful image (NobelPrize.org., Stockholm, Sweden) (available at: www.nobelprize.org/prizes/physics/2022/aspect/lecture/) (Accessed 8 December 2022)
- [20] Zeilinger A 2022 Nobel lecture: a voyage through quantum wonderland (NobelPrize.org., Stockholm, Sweden) (available at: www.nobelprize.org/prizes/physics/2022/zeilinger/lecture/) (Accessed 8 December 2022)
- [21] Clauser J 2022 Nobel Lecture: experimental proof that nonlocal quantum entanglement is real (NobelPrize.org., Stockholm, Sweden) (available at: www.nobelprize.org/prizes/physics/2022/clauzer/lecture/) (Accessed 8 December 2022)
- [22] Mandel L and Wolf E 1995 *Optical Coherence and Quantum Optics* (Cambridge University Press)
- [23] Vogel W and Welsch D-G 2006 *Quantum Optics* (Wiley-VCH)
- [24] Walls D F and Milburn G J 2010 *Quantum Optics* (Springer)
- [25] Kimble H J, Dagenais M and Mandel L 1977 Photon antibunching in resonance fluorescence *Phys. Rev. Lett.* **39** 691
- [26] Breitenbach G, Schiller S and Mlynek J 1997 Measurement of the quantum states of squeezed light *Nature* **387** 471
- [27] Lvovsky A I and Raymer M G 2009 Continuous-variable optical quantum-state tomography *Rev. Mod. Phys.* **81** 299
- [28] Bachor H and Ralph T 2019 *A Guide to Experiments in Quantum Optics* (Wiley-VCH Verlag)
- [29] D'Ariano G M Laurentis M D, Paris M G A, Porzio A and Solimeno S 2002 Quantum tomography as a tool for the characterization of optical devices *J. Opt. B: Quantum Semiclass. Opt.* **4** S127–32
- [30] Blume-Kohout R 2010 Optimal, reliable estimation of quantum states *New J. Phys.* **12** 043034
- [31] D'Auria V, Fornaro S, Porzio A, Solimeno S, Olivares S and Paris M G A 2009 Full characterization of gaussian bipartite entangled states by a single homodyne detector *Phys. Rev. Lett.* **102** 020502
- [32] Vogel K and Risken H 1989 Determination of quasiprobability distributions in terms of probability distributions for the rotated quadrature phase *Phys. Rev. A* **40** 2847–9
- [33] Larson J and Mavrogordatos T 2022 *Jaynes-Cummings Model and Its Descendants: Modern Research Directions (IOP Series in Quantum Technology)* (IOP Publishing Ltd)
- [34] Acín A *et al* 2018 The quantum technologies roadmap: a European community view *New J. Phys.* **20** 080201
- [35] Walmsley I A 2015 Quantum optics: science and technology in a new light *Science* **348** 525
- [36] Deutsch I H 2020 Harnessing the power of the second quantum revolution *PRX Quantum* **1** 020101
- [37] Leonhardt U 1997 *Measuring the Quantum State of Light (Cambridge Studies in Modern Optics)* 1st edn, ed P L Knight and A Miller (Cambridge University Press)
- [38] Andersen U L, Gehring T, Marquardt C and Leuchs G 2016 30 years of squeezed light generation *Phys. Scr.* **91** 053001
- [39] Walls D F 1983 Squeezed states of light *Nature* **306** 141
- [40] Loudon R and Knight P L 1987 Squeezed light *J. Mod. Phys.* **34** 709
- [41] Wakui K, Takahashi H, Furusawa A and Sasaki M 2007 Photon subtracted squeezed states generated with periodically poled KTiOPO_4 *Opt. Express* **15** 3568–74
- [42] Diedrich F and Walther H 1987 Nonclassical radiation of a single stored ion *Phys. Rev. Lett.* **58** 203–6
- [43] Michler P, Kiraz A, Becher C, Schoenfeld W V, Petroff P M, Zhang L, Hu E and Imamoglu A 2000 A quantum dot single-photon turnstile device *Science* **290** 2282–5

- [44] Gadway B R, Galvez E J and Zela F D 2009 Bell-inequality violations with single photons entangled in momentum and polarization *J. Phys. B* **42** 015503
- [45] Magnitskiy S , Frolovsev D, Firsov V, Gostev P, Protsenko I and Saygin M 2015 A SPDC-based source of entangled photons and its characterization *J. Russ. Laser Res.* **36** 618
- [46] Takesue H and Inoue K 2004 Generation of polarization-entangled photon pairs and violation of Bell's inequality using spontaneous four-wave mixing in a fiber loop *Phys. Rev. A* **70** 031802(R)
- [47] Vallés A , D'Ambrosio V, Hendrych M, Mičuda M, Marrucci L, Sciarrino F and Torres J P 2014 Generation of tunable entanglement and violation of a Bell-like inequality between different degrees of freedom of a single photon *Phys. Rev. A* **90** 052326
- [48] Zavatta A, Viciani S and Bellini M 2004 Quantum-to-classical transition with single-photon-added coherent states of light *Science* **306** 660–2
- [49] Ourjoumtsev A , Tualle-Brouri R, Laurat J and Grangier P 2006 Generating optical Schrödinger kittens for quantum information processing *Science* **312** 83–86
- [50] Hacker B , Weltz S, Daiss S, Shaukat A, Ritter S, Li L and Rempe G 2019 Deterministic creation of entangled atom-light Schrödinger-cat states *Nat. Photon.* **13** 110
- [51] Sychev D V *et al* 2017 Enlargement of optical Schrödinger's cat states *Nat. Photon.* **11** 379
- [52] Lewenstein M, Ciappina M F, Pisanty E, Rivera-Dean J, Stammer P, Lamprou T and Tzallas P 2021 Generation of optical Schrödinger cat states in intense laser–matter interactions *Nat. Phys.* **17** 1104
- [53] Rivera-Dean J , Lamprou T, Pisanty E, Stammer P, Ordóñez A F, Maxwell A S, Ciappina M F, Lewenstein M and Tzallas P 2022 Strong laser fields and their power to generate controllable high-photon-number coherent-state superpositions *Phys. Rev. A* **105** 033714
- [54] Gilchrist A , Nemoto K, Munro W J, Ralph T C, Glancy S, Braunstein S L and Milburn G J 2004 Schrödinger cats and their power for quantum information processing *J. Opt. B: Quantum Semiclass. Opt.* **6** S828–33
- [55] Giovannetti V, Lloyd S and Maccone L 2004 Quantum-enhanced measurements: Beating the standard quantum limit *Science* **306** 1330
- [56] Giovannetti V, Lloyd S and Maccone L 2011 Advances in quantum metrology *Nat. Photon.* **5** 222
- [57] Jouguet P , Kunz-Jacques S, Leverrier A, Grangier P and Diamanti E 2013 Experimental demonstration of long-distance continuous-variable quantum key distribution *Nat. Photon.* **7** 378
- [58] Lloyd S and Braunstein S L 1999 Quantum computation over continuous variables *Phys. Rev. Lett.* **82** 1784
- [59] Ralph T C , Gilchrist A, Milburn G J, Munro W J and Glancy S 2003 Quantum computation with optical coherent states *Phys. Rev. A* **68** 042319
- [60] Joo J, Munro W J and Spiller T P 2011 Quantum metrology with entangled coherent states *Phys. Rev. Lett.* **107** 083601
- [61] Schnabel R 2017 Squeezed states of light and their applications in laser interferometers *Phys. Rep.* **684** 1
- [62] Maiman T H 1960 Stimulated optical radiation in ruby *Nature* **187** 493
- [63] McClung F J and Hellwarth R W 1962 Giant optical pulsations from ruby *J. Appl. Phys.* **33** 828
- [64] DeMaria A, Stetser D A and Heynau H 1966 Self mode-locking of lasers with saturable absorbers *Appl. Phys. Lett.* **8** 174
- [65] Delone N B and Krainov V P 2000 *Multiphoton Processes in Atoms* (*Springer Series on Atomic, Optical and Plasma Physics* vol 2000) 2nd edn (Springer)
- [66] Moulton P F 1986 Spectroscopic and laser characteristics of Ti:Al₂O₃ *J. Opt. Soc. Am. B* **3** 125
- [67] Fork R L , Brito Cruz C H, Becker P C and Shank C V 1987 Compression of optical pulses to six femtoseconds by using cubic phase compensation *Opt. Lett.* **12** 483
- [68] Zewail A H 1999 Nobel Lecture: Femtochemistry, atomic-scale dynamics of the chemical bond using ultrafast lasers (NobelPrize.org., Stockholm, Sweden) (Accessed 8 December 1999) (available at: www.nobelprize.org/prizes/chemistry/1999/zewail/lecture/)
- [69] Protopapas M, Keitel C H and Knight P L 1997 Atomic physics with super-high intensity lasers *Rep. Prog. Phys.* **60** 389
- [70] Kulander K C, Schafer K J and Krause J L 1993 Dynamics of short-pulse excitation, ionization and harmonic conversion *Super-Intense Laser Atom Physics (Nato Advanced Studies Institute Series B: Physics* vol 316), ed B Piraux, A L'Huillier and K Rzżewski (Plenum) pp 95–110
- [71] Corkum P B 1993 Plasma perspective on strong field multiphoton ionization *Phys. Rev. Lett.* **71** 1994
- [72] Lewenstein M, Balco P, Ivanov M Y, L'Huillier A and Corkum P B 1994 Theory of high-harmonic generation by low-frequency laser fields *Phys. Rev. A* **49** 2117
- [73] Ferray M , L'Huillier A, Li X F, Lompre L A, Mainfray G and Manus C 1988 Multiple-harmonic conversion of 1064 nm radiation in rare gases *J. Phys. B: At. Mol. Opt. Phys.* **21** L31
- [74] Li X F, L'Huillier A, Ferray M, Lompré L A and Mainfray G 1989 Multiple-harmonic generation in rare gases at high laser intensity *Phys. Rev. A* **39** 5751
- [75] Gohle C , Udem T, Herrmann M, Rauschenberger J, Holzwarth R, Schuessler H A, Krausz F and Hänsch T W 2005 A frequency comb in the extreme ultraviolet *Nature* **436** 234
- [76] Cingöz A , Yost D C, Allison T K, Ruehl A, Fermann M E, Hartl I and Ye J 2012 Direct frequency comb spectroscopy in the extreme ultraviolet *Nature* **482** 68
- [77] Krausz F and Ivanov M 2009 Attosecond physics *Rev. Mod. Phys.* **81** 163
- [78] Corkum P B and Krausz F 2007 Attosecond science *Nat. Phys.* **3** 381
- [79] Reduzzi M *et al* 2015 Advances in high-order harmonic generation sources for time-resolved investigations *J. Electron Spectrosc. Relat. Phenom.* **204** 257
- [80] Borrego-Varillas R, Lucchini M and Nisoli M 2022 Attosecond spectroscopy for the investigation of ultrafast dynamics in atomic, molecular and solid-state physics *Rep. Prog. Phys.* **85** 066401
- [81] Chatzithanasiou S , Kahaly S, Skantzakis E, Sansone G, Lopez-Martens R, Haessler S, Varju K, Tsakiris G, Charalambidis D and Tzallas P 2017 Generation of attosecond light pulses from gas and solid state media *Photonics* **4** 26
- [82] Orfanos I , Makos I, Lontos I, Skantzakis E, Förög B, Charalambidis D and Tzallas P 2019 Attosecond pulse metrology *APL Photon.* **4** 080901
- [83] Amini K *et al* 2019 Symphony on strong field approximation *Rep. Prog. Phys.* **82** 116001
- [84] LaGattuta K J 1993 Radiation emitted by a resonantly driven hydrogen atom *Phys. Rev. A* **48** 666
- [85] Wang Y B, Guo Y, Chen J, Yan Z-C and Fu P 2012 Frequency-domain theory of nonsequential double ionization in intense laser fields based on nonperturbative QED *Phys. Rev. A* **85** 023402
- [86] Yangliev D N, Krainov V P and Tolstikhin O I 2020 Quantum theory of radiation by nonstationary systems with application to high-order harmonic generation *Phys. Rev. A* **101** 013410
- [87] Gauthey F I , Keitel C H, Knight P L and Maquet A 1995 Role of initial coherence in the generation of harmonics

- and sidebands from a strongly driven two-level atom *Phys. Rev. A* **52** 525
- [88] Gombkötő A *et al* 2020 High-order harmonic generation as induced by a quantized field: Phase-space picture *Phys. Rev. A* **101** 013418
- [89] Varró S 2021 Quantum optical aspects of high-harmonic generation *Photonics* **8** 269
- [90] Gao J, Shen F and Eden J G 2000 Interpretation of high order harmonic generation in terms of transitions between quantum Volkov states *Phys. Rev. A* **61** 043812
- [91] Hu H and Yuan J 2008 Time-dependent QED model for high order harmonic generation in ultrashort intense laser pulses *Phys. Rev. A* **78** 063826
- [92] Fu P, Wang B, Li X and Gao L 2001 Interrelation between high-order harmonic generation and above-threshold ionization *Phys. Rev. A* **64** 063401
- [93] Kuchiev M Y and Ostrovsky V N 1999 Quantum theory of high harmonic generation via above-threshold ionization and stimulated recombination *J. Phys. B: At. Mol. Opt. Phys.* **32** L189
- [94] Usachenko V I and Pazdzersky V A 2002 High-order harmonic generation in a strong laser field: an alternative quantum-mechanical model *J. Phys. B: At. Mol. Opt. Phys.* **35** 761
- [95] Bogatskaya A V, Volkova E A and Popov A M 2017 Spontaneous emission of atoms in a strong laser field *J. Exp. Theor. Phys.* **125** 587
- [96] Burenkov I A and Tikhanova O V 2010 Features of multiphoton-stimulated bremsstrahlung in a quantized field *J. Phys. B: At. Mol. Opt. Phys.* **43** 235401
- [97] Gorlach A , Neufeld O, Rivera N, Cohen O and Kaminer I 2020 The quantum-optical nature of high harmonic generation *Nat. Commun.* **11** 4598
- [98] Stammer P , Rivera-Dean J, Maxwell A, Lamprou T, Ordóñez A, Ciappina M F, Tzallas P and Lewenstein M 2023 Quantum electrodynamics of intense laser-matter interactions: A tool for quantum state engineering *PRX Quantum* **4** 010201
- [99] Gonoskov I A , Tsatsrafyllis N, Kominis I K and Tzallas P 2016 Quantum optical signatures in strong-field laser physics: infrared photon counting in high-order harmonic generation *Sci. Rep.* **6** 32821
- [100] Tsatsrafyllis N , Kominis I K, Gonoskov I A and Tzallas P 2017 High-order harmonics measured by the photon statistics of the infrared driving-field exiting the atomic medium *Nat. Commun.* **8** 15170
- [101] Tsatsrafyllis N *et al* 2019 Quantum optical signatures in a strong laser pulse after interaction with semiconductors *Phys. Rev. Lett.* **122** 193602
- [102] Stammer P 2022 Theory of entanglement and measurement in high-order harmonic generation *Phys. Rev. A* **106** L050402
- [103] Stammer P , Rivera-Dean J, Lamprou T, Pisanty E, Ciappina M F, Tzallas P and Lewenstein M 2022 High photon number entangled states and coherent state superposition from the extreme ultraviolet to the far infrared *Phys. Rev. Lett.* **128** 123603
- [104] Rivera-Dean J , Stammer P, Pisanty E, Lamprou T, Tzallas P, Lewenstein M and Ciappina M F 2021 New schemes for creating large optical Schrödinger cat states using strong laser fields *J. Comput. Electron.* **20** 2111
- [105] Rivera-Dean J , Stammer P, Maxwell A S, Lamprou T, Tzallas P, Lewenstein M and Ciappina M F 2022 Light-matter entanglement after above-threshold ionization processes in atoms *Phys. Rev. A* **106** 063705
- [106] Gerry C and Knight P 2005 *Introductory Quantum Optics* (Cambridge University Press)
- [107] Leonhardt U 2010 *Essential Quantum Optics* (Cambridge University Press)
- [108] Scully M O and Zubairy M S 2010 *Quantum Optics* (Cambridge University Press)
- [109] Lambropoulos P and Petrosyan D 2007 *Fundamentals of Quantum Optics and Quantum Information* (Springer)
- [110] Schleich W P 2001 *Quantum Optics in Phase Space* (Wiley-VCH Verlag)
- [111] Strekalov D V and Leuchs G 2019 Nonlinear Interactions and non-Classical Light *Quantum Photonics: Pioneering Advances and Emerging Applications* ed R W Boyd, S G Lukishova and V N Zadkov (Springer) p 51
- [112] Herman G T 1980 *Image Reconstruction From Projections: The Fundamentals of Computerized Tomography* (Academic)
- [113] Lvovsky A I 2004 Iterative maximum-likelihood reconstruction in quantum homodyne tomography *J. Opt. B: Quantum Semiclass. Opt.* **6** S556
- [114] Moerner W E and Kador L 1989 Optical detection and spectroscopy of single molecules in a solid *Phys. Rev. Lett.* **62** 2535
- [115] Aharonovich I, Englund D and Toth M 2016 Solid-state single-photon emitters *Nat. Photon.* **10** 631
- [116] Castelletto S , Johnson B C, Ivády V, Stavrias N, Umeda T, Gali A and Ohshima T 2014 A silicon carbide room-temperature single-photon source *Nat. Mater.* **13** 151
- [117] Branny A , Kumar S, Proux R and Gerardot B D 2017 Deterministic strain-induced arrays of quantum emitters in a two-dimensional semiconductor *Nat. Commun.* **8** 15053
- [118] Haroche S and Raimond J-M 2006 *Exploring the Quantum: Atoms, Cavities and Photons* (Oxford University Press Inc.)
- [119] Schrödinger E 1935 Die gegenwärtige situation in der quantenmechanik *Naturwissenschaften* **23** 844
- [120] Ourjoumtsev A , Jeong H, Tualle-Brouri R and Grangier P 2007 Generation of optical ‘Schrödinger cats’ from photon number states *Nature* **448** 784–6
- [121] Dakna M , Anhut T, Opatrný T, Knöll L and Welsch D-G 1997 Generating Schrödinger-cat-like states by means of conditional measurements on a beam splitter *Phys. Rev. A* **55** 3184
- [122] Horodecki R , Horodecki P, Horodecki M and Horodecki K 2009 Quantum entanglement *Rev. Mod. Phys.* **81** 865
- [123] Einstein A, Podolsky B and Rosen N 1935 Can quantum-mechanical description of physical reality be considered complete? *Phys. Rev.* **47** 777
- [124] Reid M , Drummond P D, Bowen W P, Cavalcanti E G, Lam P K, Bachor H A, Andersen U L and Leuchs G 2009 Colloquium: the Einstein–Podolsky–Rosen paradox: from concepts to applications *Rev. Mod. Phys.* **81** 1727
- [125] Sanders B C 2012 Review of entangled coherent states *J. Phys. A: Math. Theor.* **45** 244002
- [126] Sanders B C 1992 Entangled coherent states *Phys. Rev. A* **45** 6811
- [127] van Enk S J and Hirota O 2001 Entangled coherent states: Teleportation and decoherence *Phys. Rev. A* **64** 022313
- [128] Nolte S, Schremppel F and Dausinger F 2016 *Ultrashort Pulse Laser Technology Laser Sources and Applications* (*Springer Series in Optical Sciences* vol 195) (Springer International Publishing)
- [129] Backus S , Durfee C G, Murnane M M and Kapteyn H C 1998 High power ultrafast lasers *Rev. Sci. Instr.* **69** 1207
- [130] Steinmeyer G , Sutter D H, Gallmann L, Matuschek N and Keller U 1999 Frontiers in ultrashort pulse generation: pushing the limits in linear and nonlinear optics *Science* **286** 1507
- [131] Baltuška A *et al* 2003 Attosecond control of electronic processes by intense light fields *Nature* **421** 611–5
- [132] Kühn S *et al* 2017 The ELI-ALPS facility: the next generation of attosecond sources *J. Phys. B: At. Mol. Opt. Phys.* **50** 132002

- [133] Biegert J, Bates P K and Chalus O 2011 New mid-infrared light sources *IEEE J. Sel. Top. Quantum Electron.* **18** 531
- [134] Andriukaitis G , Balčiunas T, Ališauskas S, Pugžlys A, Baltuška A, Popmintchev T, Chen M-C, Murnane M M and Kapteyn H C 2011 90 GW peak power few-cycle mid-infrared pulses from an optical parametric amplifier *Opt. Lett.* **36** 2755
- [135] Fan G , Balčiunas T, Kanai T, Flöry T, Andriukaitis G, Schmidt B E, Légaré F and Baltuška A 2016 Hollow-core-waveguide compression of multi-millijoule cep-stable 3.2- μ m pulses *Optica* **3** 1308
- [136] Steinleitner P *et al* 2022 Single-cycle infrared waveform control *Nat. Photon.* **16** 512–8
- [137] Hebling J , Yeh K-L, Hoffmann M C, Bartal B and Nelson K A 2008 Generation of high-power terahertz pulses by tilted-pulse-front excitation and their application possibilities *J. Opt. Soc. Am. B* **25** B6
- [138] Gollner C , Shalaby M, Brodeur C, Astrauskas I, Jutas R, Constable E, Bergen L, Baltuška A and Pugžlys A 2021 Highly efficient thz generation by optical rectification of mid-ir pulses in dast *APL Photonics* **6** 046105
- [139] Keldysh L 1965 Ionization in the field of a strong electromagnetic wave *Sov. Phys. JETP* **20** 1307
Keldysh L 1965 *Zh. Eksp. Teor. Fiz.* **47** 1945
- [140] Perelomov A, Popov V and Terent'ev M 1966 Ionization of atoms in an alternating electric field *Sov. Phys. JETP* **23** 924
Perelomov A, Popov V and Terent'ev M 1966 *Zh. Eksp. Teor. Fiz.* **50** 1393
- [141] Reiss H R 1980 Effect of an intense electromagnetic field on a weakly bound system *Phys. Rev. A* **22** 1786
- [142] Ammosov M, Delone N and Krainov V 1986 Tunnel ionization of complex atoms and of atomic ions in an alternating electromagnetic field *Sov. Phys. JETP* **64** 1191
Ammosov M, Delone N and Krainov V 1986 *Zh. Eksp. Teor. Fiz.* **91** 2008
- [143] Faisal F H M 2016 *Theory of Multiphoton Processes* vol 195 (Springer)
- [144] Agostini P, Fabre F, Mainfray G, Petite G and Rahman N K 1979 Free-free transitions following six-photon ionization of xenon atoms *Phys. Rev. Lett.* **42** 1127
- [145] Chin S L, Yergeau F and Lavigne P 1985 Tunnel ionisation of Xe in an ultra-intense CO₂ laser field (10^{14} W cm⁻²) with multiple charge creation *J. Phys. B: At. Mol. Phys.* **18** L213
- [146] Faisal F H 1973 Multiple absorption of laser photons by atoms *J. Phys. B: At. Mol. Phys.* **6** L89
- [147] Lewenstein M , Kulander K C, Schafer K J and Bucksbaum P H 1995 Rings in above-threshold ionization: A quasiclassical analysis *Phys. Rev. A* **51** 1495
- [148] Becker W, Lohr A and Kleber M 1995 Light at the End of the tunnel: Two- and three-step models in intense-field laser-atom physics *Quantum Semiclass. Opt.* **7** 423
- [149] Armstrong G S J , Khokhlova M A, Labeye M, Maxwell A S, Pisanty E and Ruberti M 2021 Dialogue on analytical and ab initio methods in attoscience *Eur. Phys. J. D* **75** 209
- [150] Paulus G G , Nicklich W, Xu H, Lambropoulos P and Walther H 1994 Plateau in above threshold ionization spectra *Phys. Rev. Lett.* **72** 2851
- [151] Pullen M G *et al* 2015 Imaging an aligned polyatomic molecule with laser-induced electron diffraction *Nat. Commun.* **6** 7262
- [152] Wolter B *et al* 2016 Ultrafast electron diffraction imaging of bond breaking in di-ionized acetylene *Science* **354** 308
- [153] Huismans Y *et al* 2011 Time-resolved holography with photoelectrons *Science* **331** 61
- [154] de Morisson Faria C F and Maxwell A S 2020 It is all about phases: ultrafast holographic photoelectron imaging *Rep. Prog. Phys.* **83** 034401
- [155] Pisanty E, Ciappina M F and Lewenstein M 2020 The imaginary part of the high-harmonic cutoff *J. Phys. Photon.* **2** 034013
- [156] McPherson A , Gibson G, Jara H, Johann U, Luk T S, McIntyre I A, Boyer K and Rhodes C K 1987 Studies of multiphoton production of vacuum-ultraviolet radiation in the rare gases *J. Opt. Soc. Am. B* **4** 595
- [157] Salières P *et al* 1999 Study of the spatial and temporal coherence of high-order harmonics *Adv. At. Mol. Opt. Phys.* **41** 83
- [158] Lewenstein M and L'Huillier A 2008 Principles of single atom physics: High-order harmonic generation, above-threshold ionization and non-sequential ionization *Strong Field Laser Physics* (Springer) p 147
- [159] Weissenbilder R, Carlström S, Rego L, Guo C, Heyl C M, Smorenburg P, Constant E, Arnold C L and L'Huillier A 2022 How to optimize high-order harmonic generation in gases *Nat. Rev. Phys.* **4** 713
- [160] Khokhlova M A and Strelkov V V 2020 Highly efficient XUV generation via high-order frequency mixing *New J. Phys.* **22** 093030
- [161] Johnson A S *et al* 2018 High-flux soft x-ray harmonic generation from ionization-shaped few-cycle laser pulses *Sci. Adv.* **4** eaar3761
- [162] Popmintchev T, Chen M-C, Cohen O, Grisham M E, Rocca J J, Murnane M M and Kapteyn H C 2008 Extended phase matching of high harmonics driven by mid-infrared light *Opt. Lett.* **33** 2128
- [163] Perry M D and Crane J K 1993 High-order harmonic emission from mixed fields *Phys. Rev. A* **48** R4051
- [164] Bertrand J B , Wörner H J, Bandulet H-C, Bisson É, Spanner M, Kieffer J-C, Villeneuve D M and Corkum P B 2011 Ultrahigh-order wave mixing in noncollinear high harmonic generation *Phys. Rev. Lett.* **106** 023001
- [165] Fleischer A , Kfir O, Diskin T, Sidorenko P and Cohen O 2014 Spin angular momentum and tunable polarization in high-harmonic generation *Nat. Photon.* **8** 543
- [166] Pisanty E, Sukiasyan S and Ivanov M 2014 Spin conservation in high-order-harmonic generation using bicircular fields *Phys. Rev. A* **90** 043829
- [167] Zürch M, Kern C, Hansinger P, Dreischuh A and Spielmann C 2012 Strong-field physics with singular light beams *Nat. Phys.* **8** 743
- [168] Hernández-García C , Picón A, San Román J and Plaja L 2013 Attosecond extreme ultraviolet vortices from high-order harmonic generation *Phys. Rev. Lett.* **111** 083602
- [169] Pisanty E , Rego L, San Román J, Picón A, Dorney K M, Kapteyn H C, Murnane M M, Plaja L, Lewenstein M and Hernández-García C 2019 Conservation of torus-knot angular momentum in high-order harmonic generation *Phys. Rev. Lett.* **122** 203201
- [170] Chipperfield L E , Robinson J S, Tisch J W G and Marangos J P 2009 Ideal waveform to generate the maximum possible electron recollision energy for any given oscillation period *Phys. Rev. Lett.* **102** 063003
- [171] Haessler S *et al* 2014 Optimization of quantum trajectories driven by strong-field waveforms *Phys. Rev. X* **4** 021028
- [172] Jin C, Wang G, Wei H, Le A-T and Lin C D 2014 Waveforms for optimal sub-keV high-order harmonics with synthesized two- or three-colour laser fields *Nat. Commun.* **5** 4003
- [173] Kfir O , Bordo E, Ilan Haham G, Lahav O, Fleischer A and Cohen O 2016 In-line production of a bi-circular field for generation of helically polarized high-order harmonics *Appl. Phys. Lett.* **108** 211106
- [174] Ganeev R A , Strelkov V V, Hutchison C, Zaïr A, Kilbane D, Khokhlova M A and Marangos J P 2012 Experimental and theoretical studies of two-color-pump resonance-induced

- enhancement of odd and even harmonics from a tin plasma *Phys. Rev. A* **85** 023832
- [175] Strelkov V V, Khokhlova M A and Shubin N Y 2014 High-order harmonic generation and fano resonances *Phys. Rev. A* **89** 053833
- [176] Khokhlova M A , Emelin M Y, Ryabikin M Y and Strelkov V V 2021 Polarization control of quasimonochromatic XUV light produced via resonant high-order harmonic generation *Phys. Rev. A* **103** 043114
- [177] Rego L *et al* 2019 Generation of extreme-ultraviolet beams with time-varying orbital angular momentum *Science* **364** eaaw9486
- [178] L'Huillier A , Lompre L A, Mainfray G and Manus C 1983 Multiply charged ions induced by multiphoton absorption in rare gases at $0.53 \mu\text{m}$ *Phys. Rev. A* **27** 2503
- [179] Walker B , Sheehy B, DiMauro L F, Agostini P, Schafer K J and Kulander K C 1994 Precision measurement of strong field double ionization of Helium *Phys. Rev. Lett.* **73** 1227
- [180] Moshammer R *et al* 2000 Momentum distributions of Ne^{n+} ions created by an intense ultrashort laser pulse *Phys. Rev. Lett.* **84** 447
- [181] Weber T, Giessen H, Weckenbrock M, Urbasch G, Staudte A, Spielberger L, Jagutzki O, Mergel V, Vollmer M and Dörner R 2000 Correlated electron emission in multiphoton double ionization *Nature* **405** 658
- [182] Maxwell A S, Madsen L B and Lewenstein M 2022 Entanglement of orbital angular momentum in non-sequential double ionization *Nat. Commun.* **13** 4706
- [183] Bauer D and Koval P 2006 QPROP: a Schrödinger-solver for intense laser-atom interaction *Comput. Phys. Commun.* **174** 396
- [184] Sundaram B and Milonni P W 1990 High-order Harmonic generation: simplified model and relevance of single-atom theories to experiment *Phys. Rev. A* **41** 6571
- [185] Agarwal G S and Biswas A 2005 Quantitative measures of entanglement in pair-coherent states *J. Opt. B: Quantum Semiclass. Opt.* **7** 350
- [186] Berrada K , Abdel-Khalek S, Eleuch H and Hassouni Y 2013 Beam splitting and entanglement generation: excited coherent states *Quantum Inf. Process.* **12** 69
- [187] Kim I J , Kim C M, Kim H T, Lee G H, Lee Y S, Park J Y, Cho D J and Nam C H 2005 Highly efficient high-Harmonic generation in an orthogonally polarized two-color laser field *Phys. Rev. Lett.* **94** 243901
- [188] Mauritsson J , Johnsson P, Gustafsson E, L'Huillier A, Schafer K J and Gaarde M B 2006 Attosecond pulse trains generated using two color laser fields *Phys. Rev. Lett.* **97** 013001
- [189] Madsen L B 2021 Strong-field approximation for high-order Harmonic generation in infrared laser pulses in the accelerated Kramers-Henneberger frame *Phys. Rev. A* **104** 033117
- [190] Nielsen M A and Chuang I L 2010 *Quantum Computation and Quantum Information: 10th Anniversary Edition* (Cambridge University Press)
- [191] Plenio M B and Virmani S 2007 An introduction to entanglement measures *Quantum Inf. Comput.* **7** 1–51
- [192] van Loock P 2011 Optical hybrid approaches to quantum information *Laser Photon. Rev.* **5** 167
- [193] Milošević D B *et al* 2006 Above-threshold ionization by few-cycle pulses *J. Phys. B: At. Mol. Opt. Phys.* **39** R203
- [194] Ciappina M F *et al* 2017 Attosecond physics at the nanoscale *Rep. Prog. Phys.* **80** 054401
- [195] Nayak A *et al* 2019 Saddle point approaches in strong field physics and generation of attosecond pulses *Phys. Rep.* **833** 1
- [196] Alcalà J *et al* 2022 High-harmonic spectroscopy of quantum phase transitions in a high-Tc superconductor *Proc. Natl Acad. Sci.* **119** e2207766119
- [197] Pizzi A , Gorlach A, Rivera N, Nunnenkamp A and Kammerer I 2023 Light emission from strongly driven many-body systems *Nat. Phys.* **19** 551
- [198] Gonoskov I *et al* 2022 Nonclassical light generation and control from laser-driven semiconductor intraband excitations (arXiv:2211.06177)
- [199] Rivera-Dean J *et al* 2022 Quantum optical analysis of high-harmonic generation in solids within a Wannier-Bloch picture (arXiv:2211.00033)
- [200] Brown G G *et al* 2022 A real-space perspective on dephasing in solid-state high harmonic generation (arXiv:2210.16889)
- [201] Silva R E F, Blinov I V, Rubtsov A N, Smirnova O and Ivanov M 2018 High-harmonic spectroscopy of ultrafast many-body dynamics in strongly correlated systems *Nat. Photon.* **12** 266
- [202] Lamprou T *et al* 2021 Quantum-optical spectrometry in relativistic laser-plasma interactions using the high-harmonic generation process: a proposal *Photonics* **8** 192
- [203] Manceau M , Spasibko K Y, Leuchs G, Filip R and Chekhova M V 2019 Indefinite-mean pareto photon distribution from amplified quantum noise *Phys. Rev. Lett.* **123** 123606
- [204] Spasibko K Y *et al* 2017 Multiphoton effects enhanced due to ultrafast photon-number fluctuations *Phys. Rev. Lett.* **119** 223603
- [205] Mouloudakis G and Lambropoulos P 2020 Pairing superbunching with compounded nonlinearity in a resonant transition *Phys. Rev. A* **102** 023713
- [206] Lamprou T, Lontos I, Papadakis N C and Tzallas P 2020 A perspective on high photon flux nonclassical light and applications in nonlinear optics *High Power Laser Sci. Eng.* **8** e42
- [207] Tzur M E , Birk M, Gorlach A, Krüger M, Kammerer I and Cohen O 2023 Photon-statistics force in ultrafast electron dynamics *Nat. Photon.* **17** 501
- [208] Tzallas P 2023 Squeezed light effect *Nat. Photon.* **17** 463
- [209] Preskill J 2018 Quantum Computing in the NISQ era and beyond *Quantum* **2** 79
- [210] Georgescu I M, Ashhab S and Nori F 2014 Quantum simulation *Rev. Mod. Phys.* **86** 153
- [211] Fraxanet J, Salamon T and Lewenstein M 2022 The coming decades of quantum simulation (arXiv:2204.08905)
- [212] Farhi E , Goldstone J, Gutmann S, Lapan J, Lundgren A and Preda D 2001 A quantum adiabatic evolution algorithm applied to random instances of an NP-complete problem *Science* **292** 472
- [213] Gisin N and Thew R 2007 Quantum communication *Nat. Photon.* **1** 165
- [214] Degen C L, Reinhard F and Cappellaro P 2017 Quantum sensing *Rev. Mod. Phys.* **89** 035002
- [215] Baldelli N , Bhattacharya U, González-Cuadra D, Lewenstein M and Graß T 2022 Detecting Majorana zero modes via strong field dynamics *ACS Omega* **7** 47424
- [216] Bhattacharya U, Chaudhary S, Grass T, Johnson A S, Wall S and Lewenstein M 2022 Fermionic Chern insulator from twisted light with linear polarization *Phys. Rev. B* **105** L081406
- [217] Zeng B *et al* 2019 *Quantum Information Meets Quantum Matter* (Springer)
- [218] Reimann J *et al* 2018 Subcycle observation of lightwave-driven Dirac currents in a topological surface band *Nature* **562** 396
- [219] Krausz F and Stockman M I 2014 Attosecond metrology: from electron capture to future signal processing *Nat. Photon.* **8** 205
- [220] Hohenleutner M , Langer F, Schubert O, Knorr M, Huttner U, Koch S W, Kira M and Huber R 2015

- Real-time observation of interfering crystal electrons in high-harmonic generation *Nature* **523** 572
- [221] Ghimire S and Reis D A 2019 High-harmonic generation from solids *Nat. Phys.* **15** 10
- [222] Bauer D and Hansen K K 2018 High-harmonic generation in solids with and without topological edge states *Phys. Rev. Lett.* **120** 177401
- [223] Bauer C J D 2019 High-harmonic generation in Su-Schrieffer-Heeger chains *Phys. Rev. B* **99** 195428
- [224] Pattanayak A, Pujari S and Dixit G 2022 Role of Majorana fermions in high-harmonic generation from Kitaev chain *Sci. Rep.* **12** 6722
- [225] Silva R E F, Jiménez-Galán Á, Amorim B, Smirnova O and Ivanov M 2019 Topological strong-field physics on sub-laser-cycle timescale *Nat. Photon.* **13** 849
- [226] Haldane F D M 1988 Model for a quantum Hall effect without Landau levels: Condensed-matter realization of the “parity anomaly” *Phys. Rev. Lett.* **61** 2015
- [227] Jiménez-Galán A, Silva R E F, Smirnova O and Ivanov M 2020 Lightwave control of topological properties in 2D materials for sub-cycle and non-resonant valley manipulation *Nat. Photon.* **14** 728
- [228] Chacón A *et al* 2020 Circular dichroism in higher-order harmonic generation: Heralding topological phases and transitions in Chern insulators *Phys. Rev. B* **102** 134115
- [229] Goulielmakis E and Brabec T 2022 High harmonic generation in condensed matter *Nat. Photon.* **16** 411
- [230] Orthodoxou C, Zaïr A and Booth G H 2021 High harmonic generation in two-dimensional mott insulators *npj Quantum Mater.* **6** 76
- [231] Murakami Y, Takayoshi S, Koga A and Werner P 2021 High-harmonic generation in one-dimensional Mott insulators *Phys. Rev. B* **103** 035110
- [232] Murakami Y, Uchida K, Koga A, Tanaka K and Werner P 2022 Anomalous temperature dependence of high-harmonic generation in Mott insulators *Phys. Rev. Lett.* **129** 157401
- [233] Uchida K, Mattoni G, Yonezawa S, Nakamura F, Maeno Y and Tanaka K 2022 High-order harmonic generation and its unconventional scaling law in the Mott-insulating Ca_2RuO_4 *Phys. Rev. Lett.* **128** 127401
- [234] Roy A, Bera S and Saha K 2020 Nonlinear dynamical response of interacting bosons to synthetic electric field *Phys. Rev. Res.* **2** 043133
- [235] Kanega M, Ikeda T N and Sato M 2021 Linear and nonlinear optical responses in kitaev spin liquids *Phys. Rev. Res.* **3** L032024
- [236] Kleme N, Tancogne-Dejean N, Rossi G M, Yang Y, Scheiba F, Mainz R E, Di Sciacca G, Rubio A, Kärtner F X and Mücke O D 2019 Polarization-state-resolved high-harmonic spectroscopy of solids *Nat. Commun.* **10** 1319
- [237] Lovinger D, Brahlk M, Kissin P, Kennes D M, Millis A J, Engel-Herbert R and Averitt R D 2020 Influence of spin and orbital fluctuations on Mott-Hubbard exciton dynamics in LaVO_3 thin films *Phys. Rev. B* **102** 115143
- [238] Lantz G *et al* 2017 Ultrafast evolution and transient phases of a prototype out-of-equilibrium Mott–Hubbard material *Nat. Commun.* **8** 13917
- [239] Bionta M R *et al* 2021 Tracking ultrafast solid-state dynamics using high harmonic spectroscopy *Phys. Rev. Res.* **3** 023250
- [240] Johnson A S *et al* 2023 Ultrafast x-ray imaging of the light-induced phase transition in VO_2 *Nat. Phys.* **19** 215
- [241] Johnson A S *et al* 2022 Ultrafast loss of lattice coherence in the light-induced structural phase transition of V_2O_3 *Phys. Rev. Lett.* **129** 255701
- [242] Valmispild V *et al* 2022 Sub-cycle multidimensional spectroscopy of strongly correlated materials (arXiv:2208.04647)
- [243] Argenti L *et al* 2022 Atto 8th Int. Conf. on Attosecond Science and Technology (UCF) (available at: <https://sciences.ucf.edu/physics/atto/>)
- [244] Han S *et al* 2019 Extraction of higher-order nonlinear electronic response in solids using high harmonic generation *Nat. Commun.* **10** 3272
- [245] Calafell I A *et al* 2022 High-harmonic generation enhancement with graphene heterostructures *Adv. Opt. Mater.* **10** 2200715
- [246] Shao C, Lu H, Zhang X, Yu C, Tohyama T and Lu R 2022 High-harmonic generation approaching the quantum critical point of strongly correlated systems *Phys. Rev. Lett.* **128** 047401
- [247] AlShafey A *et al* 2022 Ultrafast laser-driven dynamics in metal-insulator interface (arXiv:2212.09176)
- [248] Vaswani C *et al* 2021 Light quantum control of persisting Higgs modes in iron-based superconductors *Nat. Commun.* **12** 258
- [249] Tzallas P 2023 Quantum correlated atoms in intense laser fields *Nat. Phys.* **19** 472
- [250] Cireasa R *et al* 2015 Probing molecular chirality on a sub-femtosecond timescale *Nat. Phys.* **11** 654
- [251] Ayuso D, Ordonez A F and Smirnova O 2022 Ultrafast chirality: the road to efficient chiral measurements *Phys. Chem. Chem. Phys.* **24** 26962
- [252] Ayuso D, Neufeld O, Ordonez A F, Decleva P, Lerner G, Cohen O, Ivanov M and Smirnova O 2019 Synthetic chiral light for efficient control of chiral light–matter interaction *Nat. Photon.* **13** 866
- [253] Ayuso D, Ordonez A F, Decleva P, Ivanov M and Smirnova O 2021 Enantio-sensitive unidirectional light bending *Nat. Commun.* **12** 3951
- [254] Ayuso D, Ordonez A F, Ivanov M and Smirnova O 2021 Ultrafast optical rotation in chiral molecules with ultrashort and tightly focused beams *Optica* **8** 1243
- [255] Khokhlova M, Pisanty E, Patchkovskii S, Smirnova O and Ivanov M 2022 Enantiosensitive steering of free-induction decay *Sci. Adv.* **8** eabq1962
- [256] Planas X B, Ordóñez A, Lewenstein M and Maxwell A S 2022 Ultrafast Imaging of Molecular Chirality with Photoelectron Vortices *Phys. Rev. Lett.* **129** 233201
- [257] Cavalleri A 2018 Photo-induced superconductivity *Contemp. Phys.* **59** 31
- [258] McIver J W, Schulte B, Stein F-U, Matsuyama T, Jotzu G, Meier G and Cavalleri A 2020 Light-induced anomalous Hall effect in graphene *Nat. Phys.* **16** 38
- [259] Miller T A, Chhajlany R W, Tagliacozzo L, Green B, Kovalev S, Prabhakaran D, Lewenstein M, Gensch M and Wall S 2015 Terahertz field control of in-plane orbital order in $\text{La}_{0.5}\text{Sr}_{1.5}\text{MnO}_4$ *Nat. Commun.* **6** 8175
- [260] Julià-Farré S, Dauphin A, Chhajlany R W, Grochowski P T, Wall S, Lewenstein M and Grzybowski P R 2020 Nanoscale phase separation and pseudogap in the hole-doped cuprates from fluctuating Cu-O-Cu bonds *Phys. Rev. B* **101** 125107
- [261] Pisanty E, Machado G J, Vicuña-Hernández V, Picón A, Celi A, Torres J P and Lewenstein M 2019 Knotting fractional-order knots with the polarization state of light *Nat. Photon.* **13** 569
- [262] Mayer N, Patchkovskii S, Morales F, Ivanov M and Smirnova O 2022 Imprinting chirality on atoms using synthetic chiral light fields *Phys. Rev. Lett.* **129** 243201
- [263] Even Tzur M *et al* 2022 High harmonic generation driven by quantum light ATTO 8th Int. Conf. on Attosecond Science and Technology (Book of Abstracts) (available at: <https://sciences.ucf.edu/physics/atto/book-of-abstracts/>)

- [264] Gorlach A *et al* 2022 High harmonic generation driven by quantum light (arXiv:[2211.03188](https://arxiv.org/abs/2211.03188))
- [265] Khalaf M and Kaminer I 2023 Compton scattering driven by intense quantum light *Sci. Adv.* **9** eade0932
- [266] Maxwell A S and de Morisson Faria C F 2015 Quantum interference in time-delayed nonsequential double ionization *Phys. Rev. A* **92** 023421
- [267] Maxwell A S and de Morisson Faria C F 2016 Controlling below-threshold nonsequential double ionization via quantum interference *Phys. Rev. Lett.* **116** 143001
- [268] Hao X, Chen J, Li W, Wang B, Wang X and Becker W 2014 Quantum effects in double ionization of argon below the threshold intensity *Phys. Rev. Lett.* **112** 073002
- [269] Quan W *et al* 2017 Quantum interference in laser-induced nonsequential double ionization *Phys. Rev. A* **96** 032511
- [270] Maxwell A S, Armstrong G S J, Ciappina M F, Pisanty E, Kang Y, Brown A C, Lewenstein M and Figueira de Morisson Faria C 2021 Manipulating twisted electrons in strong-field ionization *Faraday Discuss.* **228** 394
- [271] Kang Y, Pisanty E, Ciappina M, Lewenstein M, Figueira de Morisson Faria C and Maxwell A S 2021 Conservation laws for electron vortices in strong-field ionisation *Eur. Phys. J. D* **75** 199
- [272] Lewenstein M *et al* 2022 Attosecond physics and quantum information science (arXiv:[2208.14769](https://arxiv.org/abs/2208.14769))
- [273] Pabst S , Greenman L, Ho P J, Mazzotti D A and Santra R 2011 Decoherence in attosecond photoionization *Phys. Rev. Lett.* **106** 053003
- [274] Arnold C, Vendrell O and Santra R 2017 Electronic decoherence following photoionization: Full quantum-dynamical treatment of the influence of nuclear motion *Phys. Rev. A* **95** 033425
- [275] Arnold C , Larivière-Loiselle C, Khalili K, Inhester L, Welsch R and Santra R 2020 Molecular electronic decoherence following attosecond photoionisation *J. Phys. B: At. Mol. Opt. Phys.* **53** 164006
- [276] Lara-Astiaso M , Ayuso D, Tavernelli I, Decleva P, Palacios A and Martín F 2016 Decoherence, control and attosecond probing of XUV-induced charge migration in biomolecules. a theoretical outlook *Faraday Discuss.* **194** 41
- [277] Vacher M , Bearpark M J, Robb M A and Malhado J P 2017 Electron dynamics upon ionization of polyatomic molecules: coupling to quantum nuclear motion and decoherence *Phys. Rev. Lett.* **118** 083001
- [278] Vrakking M J J 2021 Control of attosecond entanglement and coherence *Phys. Rev. Lett.* **126** 113203
- [279] Koll L-M , Maikowski L, Drescher L, Witting T and Vrakking M J-J 2022 Experimental control of quantum-mechanical entanglement in an attosecond pump-probe experiment *Phys. Rev. Lett.* **128** 043201
- [280] Bustos D *et al* 2022 Probing electronic decoherence with high-resolution attosecond photoelectron interferometry *Eur. Phys. J. D* **76** 112